Two-invariant modular implicit plasticity solver framework for geomechanical simulators

Erick Slis Raggio Santos*, Eduardo Alberto de Souza Neto†

September 4, 2022

Abstract

A modular, computationally efficient integration framework for two-invariant-based elastoplastic constitutive models is proposed. It is designed to allow a range of constitutive models to be incorporated with minimal programming effort. The development is intended for efficient numerical schemes in large-scale geomechanical simulations. The modular format consists of four components: isotropic elastic relation; isotropic yield criterion; two-invariant smooth flow potential plastic flow rule; and isotropic hardening law. Linear and nonlinear bulk elasticity are considered. For the nonlinear case, a numerical assessment of the accuracy of bulk elasticity integration schemes is presented, where pure Euler and semi-analytical integrators are compared. The deviatoric component of the elastic law considers both the constant shear modulus and constant Poisson's ratio models. The combination of the classic Terzaghi compaction law with different bulk elasticity models may lead to a physical inconsistency, which is removed by a straightforward modification of the hardening law. When used in conjunction with the proposed bulk elasticity models, it results in a family of compaction laws that significantly reshape the normal compaction line – a fact that seems to have been overlooked in the literature. The main contributions concerning the plasticity integrator are: a novel integration scheme that considers the variation of specific volume within each step; and a condensed system comprising two scalar return-mapping equations. A Modified Cam-Clay model is used in the assessments. A comparison with an existing, well-known algorithm is also provided and, in spite of its modularity/generality, the proposed scheme is shown to yield significant computational gains.

Keywords: Constitutive modelling; Plasticity; Return-mapping; Geomechanics; Geomaterials.

1 Introduction

Geomechanical simulation is a invaluable tool in the Oil and Gas industry. It allows the incorporation of pore volume variations in a consistent manner in reservoir flow simulations as well as the assessment of various potential hazards associated with rock compaction [1, 2]. Reservoir rock compaction is predominantly irreversible (*plastic*) [3]. It is the main driver of strain accommodation throughout the overburden rocks and may lead to geomechanical risks and hazards associated to hydrocarbon production [4, 5, 6], such as loss of containment and seepage due to fault activation or loss of cap rock integrity; subsidence and risks to ground or seabed facilities; damage to the wellbore integrity and permeability impairment due to compaction. In this context, the ability to predict rock compaction with reasonable accuracy is crucial to the industry since, normally, no effective measures are available to remedy such consequences. Geomechanical assessments can also help improve the quality of the fluid flow simulations by history-matching the compaction and subsidence data from 3D/4D reservoir monitoring programs [7].

Irreversible straining is typically modelled by means of the mathematical theory of plasticity [8, 9, 10, 11, 12]. The modelling of plastic compaction is achieved by using plastic yield envelopes bounded in the compressive direction of the hydrostatic axis in its stress-space representation. Models such as the Modified Cam-Clay [13, 14, 15], Lade-Kim [16, 17, 18, 19], Matsuoka and Nakai [20], Mortara [21] and SR3 [22] provide a natural compaction bound with a single yield function and plastic potential. The SR4 model [23], described by two smoothly-intersecting yield surfaces, can also be represented as a single-surface model. Such models tend to be preferred in geomechanical simulations due to the relative simplicity stemming from their single-surface representation. Hydrostatically bounded plasticity models based on the Mohr-Coulomb, Hoek-Brown [24], Dimaggio-Sandler [25, 26], Drucker-Prager [27] and chalk model [28] envelopes, on the other hand, have a multi-surface representation which typically leads to greater complexity of implementation.

*Petrobras RD&I Center, Rio de Janeiro, Brazil - erick_slis@petrobras.com.br

†Department of Civil Engineering, Faculty of Science and Engineering, Swansea University - UK - e.desouzaneto@swansea.ac.uk

Geomechanical assessment usually involves a very significant computational effort. Typical problems simulating the reservoir and side-, under- and overburden strata often require spatial discretisations amounting to hundreds of millions of degrees of freedom, analysed over tens of time (or pseudo-time) steps. Also, multiple model scenarios often need to be considered to account for critical inherent uncertainties in the geological characterisation of the domain. Hence, every computational efficiency gain is highly desirable to ensure reliable simulation results can be obtained within reasonable time to support strategic decision-making. In this context, plastic integrators should be made as efficient as possible and any unnecessary complexities in the constitutive models should be avoided.

In addition, flexibility of the elastoplastic integrator framework is highly desirable to allow the implementation of a wider range of models, so that each material of the geological strata can be adequately described. While sands, friable sandstones and shales fall within the series of critical state materials like the Modified Cam-Clay, carbonate rocks may be better represented by yield envelopes composed of almost-perfect shear plasticity and hardening compaction. Stiff and fault rocks may otherwise present irrelevant irreversible compaction and hence be described by open envelopes in the hydrostatic compression direction. Depending on experimental data and the stress ranges of interest, elastic relations may be modelled as either linear or nonlinear.

This work proposes the formulation of a computationally-efficient, yet flexible, two-invariant first-order-implicit elastoplasticity solver framework for large-scale geomechanical simulations. The framework is designed in a modular format to allow a range of models to be incorporated with minimal programming effort. This feature is of particular relevance to the industry which, very often, relies on specialist software developed in-house, and complexities in the program structure will have a detrimental impact on development costs. The framework incorporates isotropic elasticity, isotropic hardening, arbitrary isotropic single-function yield criteria and smooth two-invariant-based flow potential – all leading to a radial return mapping format in the deviatoric space. Three alternative combinations of isotropic elastic relations are proposed based on linear and nonlinear bulk and deviatoric responses. A numerical assessment of the accuracy of nonlinear bulk elasticity integration schemes is presented, where purely-numerical and semi-analytical integrators are tested and compared. The integration scheme yielding the most favourable balance between computational cost and numerical accuracy is suggested. The deviatoric component of the elastic law – where both the constant shear modulus and constant Poisson's ratio models are considered – is treated in a standard fashion. Isotropic hardening is described having the plastic volumetric strain as the hardening variable – a common simple approach for geomaterials. A hardening model yielding the classical Terzaghi compaction law is used in the assessments presented in the paper, but the framework supports any isotropic law.

The effect of the combination of the classic Terzaghi compaction model with linear bulk elasticity is also discussed. It is shown that this combination may lead to a physical inconsistency. This possible inconsistency is removed by a straightforward modification of the hardening law. The modified hardening law in conjunction with the proposed bulk elasticity models results in a family of compaction laws with significant variations in shape of the normal compaction line – a fact that is fundamental to the correct experimental identification of the hardening parameter but seems to have been overlooked in the literature.

In the numerical integration of the elastic relation and hardening evolution laws, the specific volume is taken as a constant within the pseudo-time increment. However, in contrast with the common practice of using its value at the beginning of the increment, the proposed algorithm can take the specific volume at an arbitrary pseudo-time within the increment. This is a novel approach leading to a plastic integrator with mixed time schemes, including a fully implicit algorithm.

The paper is organised as follows. Section 2 reviews some fundamental relations of elastoplasticity and introduces crucial notation used in the paper. The elasticity models incorporated into the proposed scheme are described in section 3 together with the algorithms used in the integration of their corresponding rate equations. Section 4 discusses the hardening laws together with the associated numerical integration scheme. A potential inconsistency is identified in combining a generalised bulk elasticity model and the classical Terzaghi compaction law, and a simple modification of the compaction model is proposed to address the issue. Properties of the normal compaction lines associated with different combinations of hardening law and elasticity models are discussed in detail. The treatment of the overall plasticity model is addressed in section 5. A two-equation return mapping scheme, radial in the deviatoric plane, is proposed and the general explicit expressions for the associated consistent tangent constitutive operator are presented. The accuracy and performance of the scheme are assessed in section 6, where a Modified Cam-Clay model (a particular member of the family of models that can be incorporated in the proposed framework) is used as the underlying model. The assessment shows that some significant gains are achieved in comparison of a widely used scheme. Some concluding remarks are presented in section 7. The paper closes with the Appendix A, which details the algorithms for the solution of the elastoplastic constitutive problem in the proposed framework.

2 Preliminaries

The plasticity theory in two-invariant space – also known as S-space [12] or triaxial space – constitutes the basis of the proposed plastic integrator framework. In what follows, all stress quantities are *poromechanics effective stresses of Biot* [29, 30] and the same effective stress is used in the formulation of the elastic and plastic constitutive laws. In addition, the Biot-Willis coefficient is assumed to be a given constant and, therefore, does not appear explicitly in the formulation. It should be noted that strong evidence suggests that the plastic distortion under shear stress with resulting significant rock fissure evolution is best modelled by an effective stress law closer to that of Terzaghi [30]. However, under progressive compaction – the regime of interest for reservoir compaction simulation and the focus of the present paper – the effective stress of Biot is a better descriptor.

The two-invariant stress quantities are the hydrostatic (or mean) stress, p, and the von Mises or generalised shear stress, q:

$$p = \frac{1}{3} tr(\boldsymbol{\sigma}); \qquad q = \sqrt{\frac{3}{2}} \|\boldsymbol{s}\|, \tag{1}$$

where $\boldsymbol{\sigma}$ is the stress tensor and

$$\boldsymbol{s} = \boldsymbol{\sigma} - p\boldsymbol{I} \tag{2}$$

is the deviatoric stress (or shear) tensor, with $\boldsymbol{I}$ denoting the identity tensor. The classical continuum mechanics convention of tensile-positive stresses (and strains) [10, 11] is adopted here. Similarly, two infinitesimal strain invariants are defined as power-conjugates of the stress invariants: the volumetric strain,

$$\varepsilon_v = tr(\boldsymbol{\varepsilon}), \tag{3}$$

where $\boldsymbol{\varepsilon}$ is the strain tensor; and the distortional strain,

$$\varepsilon_d = \sqrt{\frac{2}{3}} \|\boldsymbol{\epsilon}\|, \tag{4}$$

where

$$\boldsymbol{\epsilon} = \boldsymbol{\varepsilon} - \frac{1}{3}\varepsilon_v \boldsymbol{I} \tag{5}$$

is the strain deviator. For convenience, the stress and strain invariants are grouped using the following notation:

$$\vec{\sigma} \equiv \begin{bmatrix} p \\ q \end{bmatrix}; \qquad \vec{\varepsilon} \equiv \begin{bmatrix} \varepsilon_v \\ \varepsilon_d \end{bmatrix}. \tag{6}$$

2.1 The elastoplastic constitutive model

The classical theory of plasticity [11] is commonly used in the formulation of geomechanical constitutive models. In this context, a rather general family of useful models can be defined relying on the following postulates:

- Additive decomposition of the strain tensor into an *elastic* and a *plastic* part:

$$\boldsymbol{\varepsilon} \equiv \boldsymbol{\varepsilon}^e + \boldsymbol{\varepsilon}^p; \tag{7}$$

- An *isotropic elastic constitutive equation* written in terms of stress and strain rates:

$$\dot{\boldsymbol{\sigma}} = \dot{p}\boldsymbol{I} + \dot{\boldsymbol{s}}, \tag{8}$$

  where the superimposed dot denotes time/pseudo-time rate. In this equation, the rates of hydrostatic and deviatoric stresses are given by

$$\dot{p} = K(p, v)\, \dot{\varepsilon}_v^e, \qquad \dot{\boldsymbol{s}} = 2G(p, v)\, \dot{\boldsymbol{\epsilon}}^e, \tag{9}$$

  with K and G denoting the instantaneous bulk and shear elastic moduli which, in general, dependent on p and the *specific volume*, v, defined as

$$v \equiv \frac{V_T}{V_S}, \tag{10}$$

  where V_T and V_S denote, respectively the bulk volume and the volume of solids. Here we shall assume absence of occluded porosity in the rock matrix. Under this assumption [30], variations of solid volume can be neglected and the rate form of (10), which together with (8, 9) will complete the definition of the rate-form elasticity constitutive law, can be written as

$$\dot{v} = v\dot{\varepsilon}_v. \tag{11}$$

- A general *isotropic yield function*, Φ, depending on the stress state[1], $\boldsymbol{\sigma}$, and a scalar *hardening thermodynamical force*, A, that defines the size of the elastic domain:

$$\Phi \equiv \Phi(\boldsymbol{\sigma}, A). \tag{12}$$

For a given A, the elastic domain is the region

$$\mathcal{E}_A = \{\boldsymbol{\sigma} \,|\, \Phi(\boldsymbol{\sigma}, A) < 0\}, \tag{13}$$

of the stress space within which no plastic flow is possible.

- A *plastic flow rule*

$$\dot{\boldsymbol{\varepsilon}}^p \equiv \dot{\gamma}\boldsymbol{N}, \tag{14}$$

where the flow vector

$$\boldsymbol{N} \equiv \frac{\partial \Psi}{\partial \boldsymbol{\sigma}}, \tag{15}$$

is the gradient of a smooth, convex flow potential

$$\Psi \equiv \Psi(\vec{\sigma}, A), \tag{16}$$

expressed in terms of the two stress invariants $\vec{\sigma}$. The flow is associative when $\Phi \equiv \Psi$.

For the class of models considered here, the flow rule can be conveniently re-written for the purpose of implementation by splitting the flow vector as

$$\boldsymbol{N} = \frac{1}{3} N_v \boldsymbol{I} + \boldsymbol{N}_{\boldsymbol{\epsilon}}, \tag{17}$$

with N_v and $\boldsymbol{N}_{\boldsymbol{\epsilon}}$ denoting its spherical and deviatoric components:

$$N_v = \frac{\partial \Psi}{\partial p}, \qquad \boldsymbol{N}_{\boldsymbol{\epsilon}} = \sqrt{\frac{3}{2}} N_d \frac{\boldsymbol{s}}{\|\boldsymbol{s}\|}, \tag{18}$$

where

$$N_d = \frac{\partial \Psi}{\partial q}. \tag{19}$$

With the above, the flow rule can be equivalently stated as

$$\dot{\varepsilon}_v^p = \dot{\gamma} N_v, \qquad \dot{\boldsymbol{\epsilon}}^p = \dot{\gamma} \boldsymbol{N}_{\boldsymbol{\epsilon}}. \tag{20}$$

The invariants-only form of the above equation reads

$$\dot{\vec{\varepsilon}}^p \equiv \begin{bmatrix} \dot{\varepsilon}_v^p \\ \dot{\varepsilon}_d^p \end{bmatrix} = \dot{\gamma} \vec{N}, \qquad \vec{N} \equiv \begin{bmatrix} N_v \\ N_d \end{bmatrix}. \tag{21}$$

- An *isotropic hardening law* defining the evolution of the scalar hardening thermodynamical force A,

$$\dot{A} \equiv H(A, v)\, \dot{\alpha}, \tag{22}$$

where H is the *generalised hardening modulus* and α is a *scalar hardening internal variable*. In geomechanical constitutive models, A and α are typically taken, respectively, as the *hydrostatic preconsolidation pressure*, p_c, and the plastic volumetric strain, ε_v^p, so that the hardening law reads

$$\dot{p}_c \equiv H(p_v, \varepsilon_v^p)\, \dot{\varepsilon}_v^p. \tag{23}$$

- Loading/unloading conditions governing the evolution of the plastic flow in (14), (20) or (21):

$$\Phi \leq 0, \qquad \dot{\gamma} \geq 0, \qquad \Phi \dot{\gamma} = 0.$$

[1] It will be presented further that the extra constraint $\Phi \equiv \Phi(\vec{\sigma}, A)$ applies when adopting a nonlinear shear elasticity model.

3 Elasticity. Models and numerical treatment

Geological materials generally present nonlinear elastic behaviour, as they tend to stiffen with progressive compression. Under certain circumstances, the elastic response may be well approximated by a linear constitutive law. Hence, it is desirable that a geomechanical solver be able to handle linear and non-linear models. In this context, three isotropic elastic models are incorporated in the framework proposed here: the linear model; a non-linear bulk elasticity model with constant shear modulus, and; a non-linear bulk elasticity model with constant Poisson's ratio. For the non-linear models, a *stiffness-shifted* variant of the Roscoe-Burland model [13] is proposed to regularise the model behaviour and allow its use under conditions of (limited) tension and low compression. We note that, without regularisation, the applicability of such models in realistic oil and gas geomechanical simulations would be severely restricted.

This section describes these non-linear models and discusses in detail the algorithms used in the integration of their corresponding rate equations. Particular attention is focussed on the accuracy of the integration algorithms, and a semi-analytical scheme is found to be an optimal choice in that, in addition to achieving higher accuracy, it avoids potential volumetric locking (unreasonably high bulk stiffness at certain states) experienced when plain Euler-based schemes are used.

3.1 Nonlinear bulk elasticity

One of the most commonly used bulk elasticity models for geomaterials was proposed by Roscoe and Burland [13]. It describes a nonlinear recoverable volumetric elastic response, represented by the swelling line [13, 14, 15, 12]

$$v = v_0 - \kappa \ln(p/p_0), \tag{24}$$

where κ is the swelling index (the gradient of the swelling line) and p_0 and v_0 are the values of p and v at a known reference state. The resulting relationship between p and v in this case is a straight line in a log-linear plot. Relation (24) implies a variable instantaneous bulk modulus in the rate form (9):

$$K(p, v) = -\frac{vp}{\kappa}. \tag{25}$$

The elasticity model defined by (25) is applicable only under strictly negative (compressive) mean stress, p. While oil and gas geomechanical simulations involve the analysis of geomaterials under predominantly compressive states, there is a need to model geomaterials under tensile mean stresses, for example, when analysing potential cap rock integrity loss – a significant threat to efficient reservoir management. In addition, it is almost inevitable that some regions of the analysed domain in regular simulations, particularly within strata near ground level/seabed, will fall under (at least small) mean tensile stresses. The stress state in such regions is typically of no relevance to the compaction simulation but robust simulators must be able to cope with such conditions so that the model/scheme will not fail under little compression or under tensile mean stresses. To address this issue, Sheng *et al.* [31] proposed a regularisation of (25) featuring a *minimum mean pressure* below which the Bulk modulus is kept constant. Sanei *et al.* [32] suggested a *pressure-shifted* variant where the mean stress in (25) is replaced with the *Cam-Clay effective mean pressure* shifted by the tensile strength p_t:

$$p^{cc} \equiv p - p_t. \tag{26}$$

With greater physical appeal, Crook *et al.* [22] proposed a bulk elasticity equation where the bulk modulus is given by

$$K^{\mathrm{SR}}(p, p_c, v) = K_0 - (1 - A)\frac{p_c}{\kappa} - A\frac{v\,p}{\kappa} \tag{27}$$

in their *SR3* plasticity model, where $0 \leq A \leq 1$ is a given constant weighting the contributions of the irrecoverable and recoverable compression to the bulk stiffness. The above elastic law is also used in the *SR4* model proposed by Prats *et al.* [23].

In the framework proposed, we shall adopt a particular instance of (26), with $A = 1$:

$$K(p, v) \equiv K_0 - \frac{v\,p}{\kappa}. \tag{28}$$

We note that by substituting (28) into $(9)_1$ and rearranging the terms, the evolution equation for p can be equivalently written as the following ordinary differential equation:

$$\frac{dp}{d\varepsilon_v^e} + \frac{v}{\kappa}p = K_0. \tag{29}$$

It is this equation that will be used later in the computational implementation of the model in the present framework.

Remark 3.1 *Equation (28) disregards the specific contribution of plastic compaction to the elastic bulk stiffening of the rock. Its adoption, however, is justified as follows. Note that, under progressive compaction, p and p_c are intrinsically related, and (28) will be able to produce similar results to those of (27) for practical purposes. In addition, the experimental identification of κ in (28) can be carried out in a relatively straightforward manner without the need to keep track of the evolution of p_c. The measurement of p_c, required if (27) is used with $A \neq 1$ instead, would add significant complexity to the experimental procedure.*

3.2 Integration of the mean stress equation

Here, we discuss the integration of the mean stress evolution equation $(9)_1$, which forms a fundamental part of the overall stress integration scheme.

Elastoplastic increments

The numerical integration of $(9)_1$ with the original non-shifted bulk modulus relation (25) of Roscoe and Burland [13] is a usual practice [33, 12], and the resulting scheme is known to be heavily sensitive to the non-linearity of the Bulk modulus. Borja [34] proposed a semi-analytical integration scheme for these equations where v is held constant at the beginning of the increment. Considering the integration between (pseudo-) time stations t_n and t_{n+1} for an elastoplastic step, this approximation leads to

$$p_{n+1}(\Delta\varepsilon_v^e) \simeq p_n e^{-\frac{v_n}{\kappa}\Delta\varepsilon_v^e}, \tag{30}$$

where

$$\Delta(\cdot) \equiv (\cdot)_{n+1} - (\cdot)_n. \tag{31}$$

For notational convenience, unless absolutely necessary, subscript $n+1$ will be suppressed in what follows to denote quantities at time station t_{n+1}. Generalised midpoint or trapezoidal-based versions of the above integration scheme can be defined as

$$p_{n+1} \simeq p_{n+1}(\Delta\varepsilon_v^e, \Delta\varepsilon_v) = p_n e^{-\frac{\bar{v}}{\kappa}\Delta\varepsilon_v^e}. \tag{32}$$

Analytical integration of (11) between pseudo-times t_n and $t_{n+\theta}$, with $\theta \in [0,1]$, gives:

$$v_{n+\theta} = v_{n+\theta}(\Delta\varepsilon_v) = v_n e^{\theta\Delta\varepsilon_v}. \tag{33}$$

The specific volume $\bar{v}$ in (32) is then defined as

$$\bar{v} \equiv \begin{cases} v_{n+\theta} & \text{(generalised midpoint case)} \\ (1-\theta)v_n + \theta v_{n+1} & \text{(generalised trapezoidal case).} \end{cases} \tag{34}$$

In the framework proposed here, we shall apply the same methodology to (29) – the regularised model $(9)_1$ with the shifted bulk modulus (28). This gives the following general mean stress update formula:

$$p\left(\Delta\varepsilon_v^e, \Delta\varepsilon_v\right) \simeq \frac{\kappa}{\bar{v}}K_0 - \left(\frac{\kappa}{\bar{v}}K_0 - p_n\right)e^{-\frac{\bar{v}}{k}\Delta\varepsilon_v^e}. \tag{35}$$

Purely elastic increments

Analytical or semi-analytical solutions can be obtained for the Roscoe-Burland and the stiffness-shifted mean stress constitutive models for purely elastic steps, i.e. when $\Delta\varepsilon_v^p = 0$ and $\Delta\varepsilon_v^e = \Delta\varepsilon_v$. These are useful for validation purposes and will be explored later to assess the accuracy of the proposed numerical integration scheme.

By combining (33), (25) and $(9)_1$, integration over $[t_n, t_{n+1}]$ gives the following analytical formula for the updated mean stress for the Roscoe-Burland model:

$$p(\Delta\varepsilon_v) = p_n e^{\frac{v_n}{\kappa}\left(1-e^{\Delta\varepsilon_v}\right)}. \tag{36}$$

For the stiffness-shifted model, in turn, only a semi-analytical integration of (29) is possible. The final expression is obtained by using the explicit Euler time-discrete form,

$$\Delta v \simeq v_n \Delta\varepsilon_v, \tag{37}$$

of (11), together with (29), and then performing the analytical integration of the resulting equation. This gives

$$p(\Delta\varepsilon_v) \simeq \frac{p_n + K_0\sqrt{\frac{\pi}{2}\frac{\kappa}{v_n}}e^{-\frac{1}{2}\frac{v_n}{\kappa}}\left\{\operatorname{erfi}\left[\sqrt{\frac{1}{2}\frac{v_n}{\kappa}}\left(1+\Delta\varepsilon_v\right)\right] - \operatorname{erfi}\left[\sqrt{\frac{1}{2}\frac{v_n}{\kappa}}\right]\right\}}{e^{\frac{1}{2}\frac{v_n}{\kappa}\Delta\varepsilon_v(2+\Delta\varepsilon_v)}}, \tag{38}$$

where $\operatorname{erfi}(\cdot)$ is the non-elementary imaginary error function.

Accuracy of integration of bulk elastic response

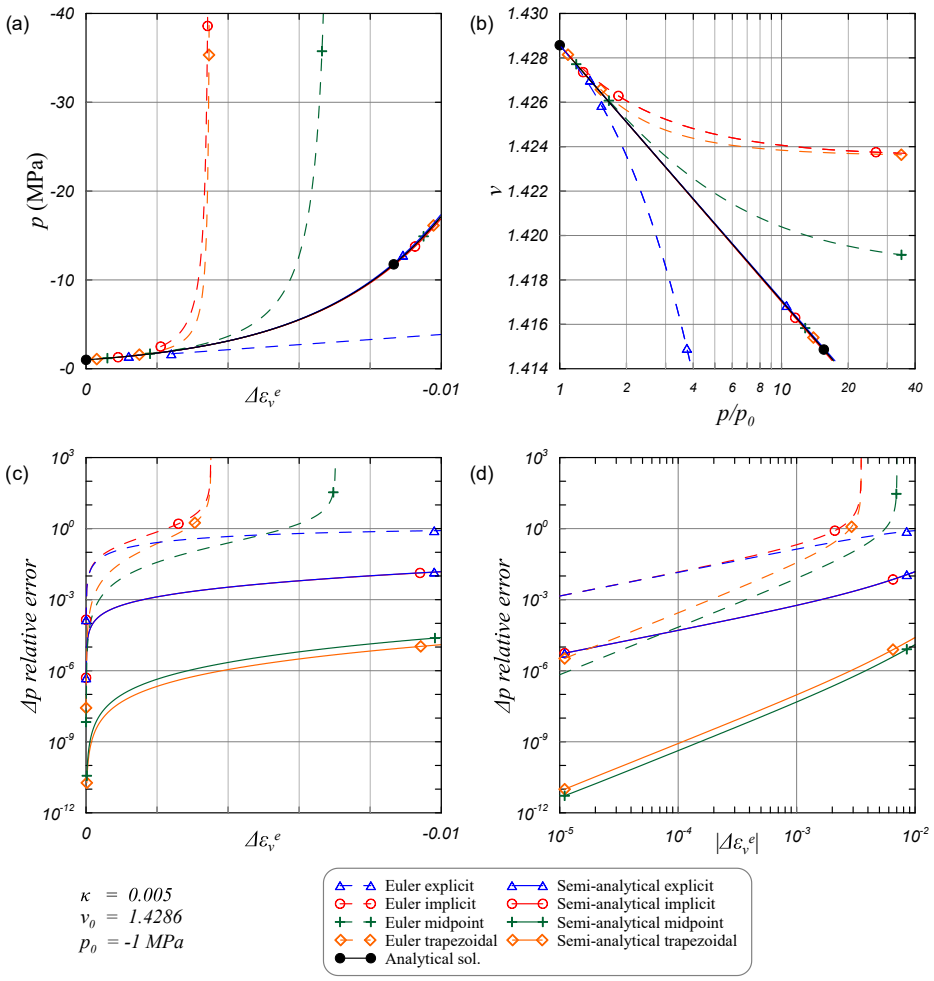

Figure 1: Numerical integration schemes for the Roscoe-Burland mean stress constitutive equation in the elastic regime. Accuracy assessment. (a) Mean stress, p, versus volumetric strain, $\Delta\varepsilon_v^e$; (b) Swelling line; (c) Relative error of mean stress integration (semi-log graph), and; (d) Relative error of mean stress integration (log-log graph).

A numerical assessment of the accuracy of the integration schemes discussed above is presented here in the elastic range. The above-suggested schemes, for both the Roscoe-Burland and the stiffness-shifted models, are tested and compared with alternative schemes based on standard first and second-order purely Euler-based methods. As will be seen, the assessment gives a clear view of the advantages of the semi-analytical schemes and provides a justification for their adoption in the geomechanical simulation framework proposed in this paper.

For each model/algorithm combination, starting from a reference state $(p, v) = (-1\text{MPa}, 1.4286)$, numerical solutions for p are obtained in single steps $\Delta\varepsilon_v^e \in [-10^{-5}, -10^{-2}]$, i.e. for compaction strain steps of 0.001% to 1%. The chosen reference state of v corresponds to a porosity of 30%. The numerical results are then plotted against the analytical solutions discussed above.

Figure 1 shows the results obtained for the Roscoe-Burland model. The corresponding purely Euler-based schemes

used for comparison are summarised below:

$$p = \begin{cases} p_n - \frac{v_n p_n}{\kappa}\Delta\varepsilon_v^e & \text{(explicit case)} \\ p_n \frac{\kappa}{\kappa + v_n e^{\Delta\varepsilon_v^e}\Delta\varepsilon_v^e} & \text{(implicit case)} \\ p_n \frac{\kappa - v_n e^{\frac{\Delta\varepsilon_v^e}{2}}\frac{\Delta\varepsilon_v^e}{2}}{\kappa + v_n e^{\frac{\Delta\varepsilon_v^e}{2}}\frac{\Delta\varepsilon_v^e}{2}} & \text{(midpoint case with } \theta = \tfrac{1}{2}) \\ \frac{1}{2}p_n\left(1 - \frac{v_n}{\kappa}\Delta\varepsilon_v^e + \frac{\kappa}{\kappa + v_n e^{\Delta\varepsilon_v^e}\Delta\varepsilon_v^e}\right) & \text{(trapezoidal case with } \theta = \tfrac{1}{2}). \end{cases} \tag{39}$$

The graph of Figure 1(a) plots the numerically integrated p against the compaction strain increment. The analytical solution is depicted in the black solid line. The corresponding relative error is defined as

$$\Delta p_{\text{rel error}} \equiv \frac{|\Delta p_{\text{num}} - \Delta p^*|}{\Delta p^*}, \tag{40}$$

where Δp^* denotes the analytical mean stress increment, is plotted in Figure 1(c). It is clear that the semi-analytical forms (other solid lines) perform significantly better than the purely Euler-based schemes, with a maximum relative error of the order of 1% for a (very large) compaction strain increment of 1% in the worst cases – the semi-analytical implicit, with $\theta = 1$ in (32), and semi-analytical explicit scheme, with $\theta = 0$. The integration error is plotted in Figure 1(d) in a log-log scale. It can be seen that the explicit-based semi-analytical scheme (30) of Borja [34] (the blue solid line) displays errors of the order of the other semi-analytical schemes. Also noteworthy is the fact that purely Euler-based implicit schemes display a potential 'volumetric locking' with greatly over-predicted mean stresses for volumetric strain increments beyond a certain size. This behaviour is the result of the form of the stress updating equations $(39)_{2\text{-}4}$ where a possible zero denominator can be obtained depending on the size of $\Delta\varepsilon_v^e$. Note, however, that for sufficiently small compaction strain increments (below about 0.2% in this example) these algorithms produce very reasonable solutions.

Figure 2 presents analogous plots for the stiffness-shifted bulk elasticity model. Model parameters have been defined to provide a significant initial stiffness $K_0 = 1\,\text{GPa}$ but with the mean stress in the same range as in the above Roscoe-Burland model assessment. The semi-analytical integrations follow expression (35) and the purely Euler-based schemes applied to this model are summarised below:

$$p = \begin{cases} p_n - \frac{v_n p_n}{\kappa}\Delta\varepsilon_v^e + K_0\Delta\varepsilon_v^e & \text{(explicit case)} \\ \frac{p_n + K_0\Delta\varepsilon_v^e}{\kappa + v_n e^{\Delta\varepsilon_v^e}\Delta\varepsilon_v^e}\kappa & \text{(implicit case)} \\ \dfrac{K_0\kappa\Delta\varepsilon_v^e + p_n\left(\kappa - v_n e^{\frac{\Delta\varepsilon_v^e}{2}}\frac{\Delta\varepsilon_v^e}{2}\right)}{\kappa + v_n e^{\frac{\Delta\varepsilon_v^e}{2}}\frac{\Delta\varepsilon_v^e}{2}} & \text{(midpoint case with } \theta = \tfrac{1}{2}) \\ \frac{p_n + K_0\Delta\varepsilon_v^e}{2}\left(1 + \frac{\kappa}{\kappa + v_n e^{\Delta\varepsilon_v^e}\Delta\varepsilon_v^e}\right) - \frac{1}{2}\frac{v_n p_n}{\kappa}\Delta\varepsilon_v^e & \text{(trapezoidal case with } \theta = \tfrac{1}{2}). \end{cases} \tag{41}$$

The graph of Figure 2(a) shows results obtained for the mean stress versus the volumetric strain increment. The analytical solution is plotted in the solid black line. The purely-Euler numerical integrations present the largest deviations, especially for the explicit and implicit schemes for $|\Delta\varepsilon_v^e|$ greater than about 0.003. In this case, no 'volumetric locking' is observed within the tested range of $\Delta\varepsilon_v^e$. However, the mean stress update formulas $(41)_{2\text{-}4}$ present similar potentially zero denominators in the implicit, midpoint and trapezoidal cases, depending on the size of $\Delta\varepsilon_v^e$. The expression of the semi-analytical integration schemes of (35), on the other hand, do not present any singularities. Figure 2(b) shows that the stiffness-shifted model produces a *curved* swelling line in the semi-log representation. This is at variance with the Roscoe-Burland model, whose semi-log representation of the swelling line is straight. This difference can be understood by noting that the specific volume expression, given by (24) for the Roscoe-Burland model, takes the form

$$v = v_0 - \kappa_{\text{eff}}\,\ln(p/p_0), \tag{42}$$

for the stiffness-shifted bulk modulus defined by (28), where

$$\kappa_{\text{eff}}(p, v) \equiv \frac{1}{\frac{1}{\kappa} - \frac{K_0}{v\,p}} \tag{43}$$

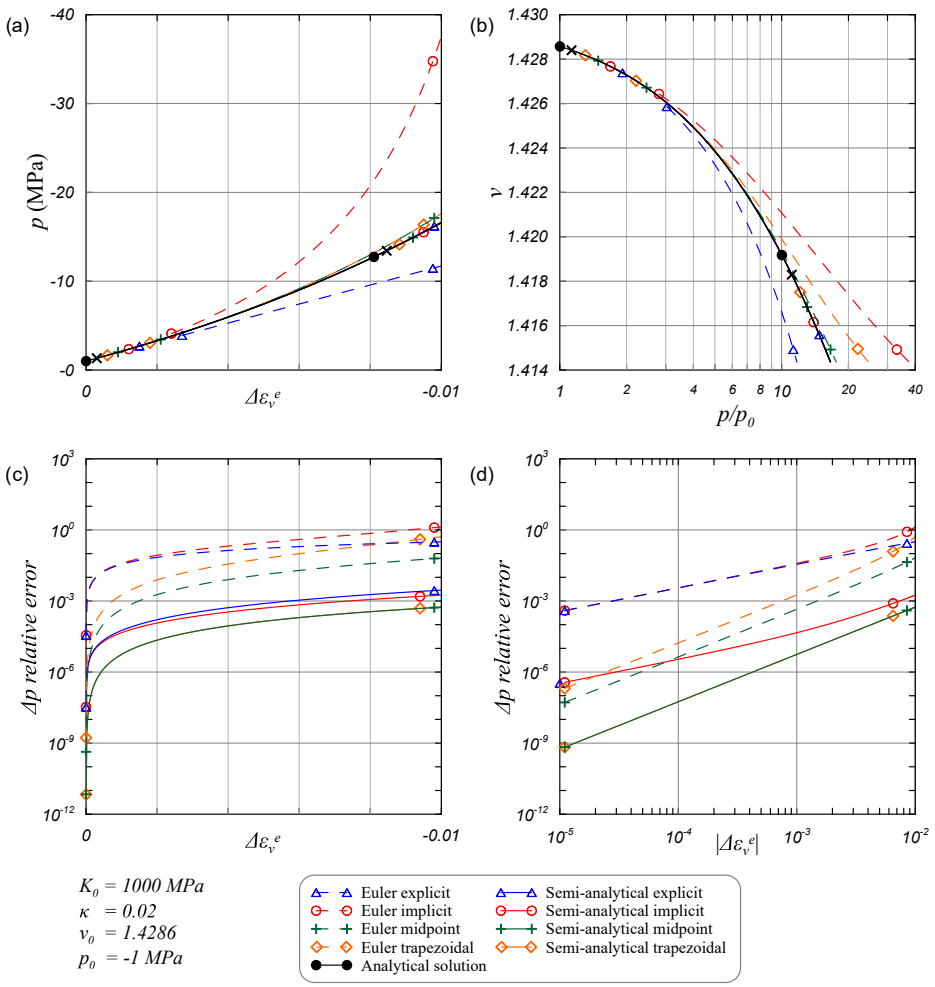

Figure 2: Numerical integration schemes for the stiffness-shifted mean stress constitutive equation in the elastic regime. Accuracy assessment. (a) Mean stress, p, versus volumetric strain, $\Delta\varepsilon_v^e$; (b) Swelling line; (c) Relative error of mean stress integration (semi-log graph), and; (d) Relative error of mean stress integration (log-log graph).

is an *effective swelling index*. The non-linearity of the swelling line in the semi-log graph stems from the second term in the denominator of the above expression – with a greater nonlinearity for low values of compressive mean stress, which decreases with increasingly compressive p.[2] We note that the nonlinearity of the swelling line for this model has experimental implications. The identification of the bulk elastic parameters – κ and K_0 in this case – can be more conveniently carried out using the K vs. vp linear plot associated with (28).

Figure 1(c) plots the relative errors of the integration schemes. Again, semi-analytical forms perform much better than the purely Euler-based schemes. In the log-log graph of 1(d) the relative integration errors become more evident. Similarly to the Roscoe-Burland model, the stiffness-shifted elastic constitutive model is best integrated using the semi-analytical schemes. In summary, all first and second-order semi-analytical integrators appear to present sufficient accuracy to be incorporated into the proposed elastoplastic framework. We note, however, that due to their simplicity, only the first-order schemes will be adopted in the present development.

[2]Note that while the stiffness-shifted model allows for tensile mean stresses, the swelling line does not have a representation under tension.

3.3 Adopted elasticity models

Classical isotropic linear elasticity implies the following relation between the Poisson's ratio, ν, the shear modulus, G, and the bulk modulus, K,

$$G = \frac{3}{2} K \frac{1-2\nu}{1+\nu}, \tag{44}$$

where ν, K and G are constants. In the modelling of geomaterials, the elastic constitutive behaviour is normally described by the rate form (9) where the bulk modulus can be a variable, such as in the bulk elasticity models discussed in the previous section. In such cases, it is common to still enforce (44) – now with variable K – and then choose to either keep constant the shear modulus (G-constant) or the Poisson's ratio (ν-constant).

In this context, it is convenient to re-write the rate form (9) in an equivalent incremental form:

$$\Delta p = \bar{K} \Delta \varepsilon_v^e, \qquad \Delta \boldsymbol{s} = 2\bar{G} \Delta \boldsymbol{\epsilon}^e, \tag{45}$$

where $\bar{G}$ and $\bar{K}$ are *secant* shear and bulk moduli, respectively. For the ν-constant variant, the following relation holds between the secant moduli [34]:

$$\bar{G} = r\bar{K}, \tag{46}$$

where

$$r \equiv \frac{3}{2} \frac{1-2\nu}{1+\nu}, \tag{47}$$

and $\bar{K}$ depends on the adopted bulk elasticity model. For the stiffness-shifted bulk elasticity model, the secant bulk modulus is found to be given by[3]

$$\bar{K}\left(\Delta \varepsilon_v^e, \Delta \varepsilon_v\right) = \frac{\kappa}{\bar{v}} \frac{K\left(p_n, \bar{v}\right) - K\left(p_{n+1}, \bar{v}\right)}{\Delta \varepsilon_v^e}. \tag{48}$$

For the linear elastic case, $\bar{K} = K$ and $\bar{G} = G$.

Remark 3.2 *The formulation of the elastic laws in terms of secant moduli is very attractive in the present context and will be adopted in the proposed elastoplastic scheme. It allows the different elastic models used in geomechanical simulations to be easily implemented within a single computational framework.*

In tensorial form, the incremental isotropic elasticity law reads

$$\Delta \boldsymbol{\sigma} = \Delta p \boldsymbol{I} + \Delta \boldsymbol{s}. \tag{49}$$

For convenience, a summary of the elasticity models incorporated in the proposed elastoplastic framework is listed in Table 1.

model	acronym	elastic moduli	
		$\bar{K}$	$\bar{G}$
linear	ILE	constant K	constant G
nonlinear bulk, G-constant	INE	$\frac{\kappa}{\bar{v}} \frac{K(p_n,\bar{v}) - K(p_{n+1},\bar{v})}{\Delta \varepsilon_v^e}$	constant G
nonlinear, ν-constant	INhE	$\frac{\kappa}{\bar{v}} \frac{K(p_n,\bar{v}) - K(p_{n+1},\bar{v})}{\Delta \varepsilon_v^e}$	$\bar{G} = r\bar{K}$

Table 1: Implemented elastic model alternatives

[3] We note that the secant modulus formula (48) retrieves the tangent modulus K for vanishingly small $\Delta \varepsilon_v^e$, i.e. $\lim_{\Delta \varepsilon_v^e \to 0} \bar{K} = K(p_n, v_n)$.

Two-invariant representation and linearisation

The representation of the adopted elastic laws in terms of stress and strain invariants will be crucial to simplify the elastoplastic integration algorithm discussed later. In the ILE model, $\Delta\boldsymbol{\sigma}$ is a function of the elastic strain exclusively and therefore can be represented as $\Delta\boldsymbol{\sigma} \equiv \Delta\boldsymbol{\sigma}(\Delta\boldsymbol{\varepsilon}^e)$. In the INE and INhE models, however, $\Delta\boldsymbol{\sigma}$ also depends on the specific volume $\bar{v}$, as can be seen in Table 1. By recalling the definition (33, 34), $\bar{v}$ is a function of the total volumetric strain, $\Delta\varepsilon_v$, in the semi-analytical elastic mean stress integration schemes with $\theta \neq 0$. Thus, the discrete stress increment, $\Delta\boldsymbol{\sigma}$, can be generally expressed as $\Delta\boldsymbol{\sigma}(\Delta\boldsymbol{\varepsilon}^e, \Delta\varepsilon_v)$ for all elastic models. The linearisation of these models will be needed in order to compute the constitutive tangent operators consistent with the adopted elastoplastic algorithms described later. Using the definition of stress and strain invariants (6), the adopted elasticity constitutive models can be linearised as

$$d\vec{\sigma} = \tilde{C}^e \, d\vec{\varepsilon}^e + \tilde{C}^t \, d\vec{\varepsilon}, \tag{50}$$

with coefficient matrices (tangent operators)

$$\tilde{C}^e \equiv \left[\frac{\partial\vec{\sigma}}{\partial\vec{\varepsilon}^e}\right], \qquad \tilde{C}^t \equiv \left[\frac{\partial\vec{\sigma}}{\partial\vec{\varepsilon}}\right] = \frac{\partial\vec{\sigma}}{\partial\bar{v}} \otimes \frac{\partial\bar{v}}{\partial\vec{\varepsilon}}. \tag{51}$$

It is convenient for the modularity of the proposed elastoplastic framework to present the expressions for $\tilde{C}^e$ and $\tilde{C}^t$ for the considered elastic constitutive models. In the ILE elasticity model these operators are constant:

$$\tilde{C}^e = \begin{bmatrix} K & 0 \\ 0 & 3G \end{bmatrix}; \qquad \tilde{C}^t = \tilde{0}, \tag{52}$$

where $\tilde{0}$ is the 2×2 zero matrix.

In the context of the nonlinear elasticity models adopted here, it suffices to present expressions for $\tilde{C}^t$ for $\theta = 0$ and $\theta = 1$. For the INE model, we have

$$\tilde{C}^e = \begin{bmatrix} K_{n+1} & 0 \\ 0 & 3G \end{bmatrix}; \qquad \tilde{C}^t = \begin{cases} \tilde{0} & \text{for } \theta = 0 \\ \bar{v}\frac{\partial\bar{K}}{\partial\bar{v}} \begin{bmatrix} \Delta\varepsilon_v^e & 0 \\ 0 & 0 \end{bmatrix} & \text{for } \theta = 1. \end{cases} \tag{53}$$

For the INhE model,

$$\tilde{C}^e = \begin{bmatrix} K_{n+1} & 0 \\ \frac{\partial q}{\partial\bar{K}}\frac{\partial\bar{K}}{\partial\Delta\varepsilon_v^e} & 3r\bar{K} \end{bmatrix}; \qquad \tilde{C}^t = \begin{cases} \tilde{0} & \text{for } \theta = 0 \\ \bar{v}\frac{\partial\bar{K}}{\partial\bar{v}} \begin{bmatrix} \Delta\varepsilon_v^e & 0 \\ 3r\Delta\varepsilon_d^e & 0 \end{bmatrix} & \text{for } \theta = 1, \end{cases} \tag{54}$$

recalling that $\bar{K} \equiv \bar{K}(\Delta\varepsilon_v^e, \Delta\varepsilon_v)$. The derivatives of $\bar{K}$ in the above are

$$\frac{\partial\bar{K}}{\partial\Delta\varepsilon_v^e} = \begin{cases} \frac{K_{n+1}-\bar{K}}{\Delta\varepsilon_v^e} & \Delta\varepsilon_v^e > 0 \\ -\frac{1}{2}\frac{\bar{v}}{\kappa}K_n & \Delta\varepsilon_v^e \approx 0 \end{cases} \tag{55}$$

and

$$\frac{\partial\bar{K}}{\partial\bar{v}} = \begin{cases} \frac{1}{\bar{v}}\left[\left(K_n + \frac{k}{\bar{v}}\frac{K_0}{\Delta\varepsilon_v^e}\right)e^{-\frac{\bar{v}}{\kappa}\Delta\varepsilon_v^e} - \frac{k}{\bar{v}}\frac{K_0}{\Delta\varepsilon_v^e}\right] & \text{for } \Delta\varepsilon_v^e > 0 \\ -\frac{p_n}{\kappa} & \text{for } \Delta\varepsilon_v^e \approx 0. \end{cases} \tag{56}$$

In the above expressions, $K_n \equiv K(p_n, v_n)$ and $K_{n+1} \equiv K(p_{n+1}, \bar{v})$. For the INhE model in (54), the expression for $\partial q/\partial\bar{K}$ in the elastic regime can be obtained as a special case of the more elaborate elastoplastic case, which will be defined later in the text.

4 Hardening law

The main purpose of the proposed elastoplastic framework is the accurate modelling of the rock compression behaviour. A reference work in the compaction of geomaterials is the *virgin* or *normal compression line* (NCL) proposed by Terzaghi

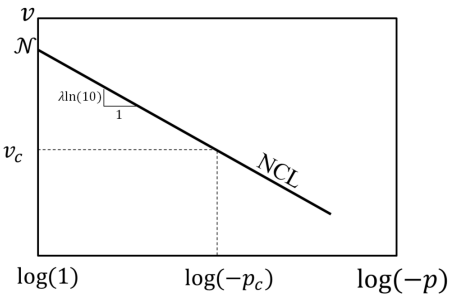

Figure 3: Terzaghi's normal compaction line

[13, 15]. It relates the specific volume, v, of the geomaterial to the *normal compaction* (or *preconsolidation*) *mean stress*, p_c, in a hydrostatic compression experiment under virgin compaction condition. As expressed by (11), the evolution of v is intrinsically related to the total volumetric strain in rate form, $\dot{\varepsilon}_v$. Hence, in the compaction model of Terzaghi alone there is no distinction between the elastic and *plastic* compression behaviours, which is necessary in an elastoplastic framework. As it will be discussed further below, when used in conjunction with the Roscoe-Burland bulk elasticity model – a usual practice – the Terzaghi model yields an isotropic hardening evolution law of the type

$$\dot{p_c} \equiv H(p_c, v)\dot{\varepsilon}_v^p, \tag{57}$$

where p_c and the volumetric plastic strain, ε_v^p, become the variables associated to hardening. In this context, p_c has the role of a thermodynamic force, ε_v^p becomes the associated internal variable and H is the experimentally-determined hardening modulus – itself a function of p_c and v.

Remark 4.1 *Given the importance of the Terzaghi compaction model and the generality provided by (57), the hardening models proposed in the present elastoplastic framework will adopt generalised rate-form evolutions of the type (57).*

In what follows, it will be shown that the Terzaghi compaction model used in conjunction with the bulk elasticity models discussed in section 3 is prone to inconsistencies under tensile mean stress regimes. The authors propose the used of an alternative expression for the hardening modulus that, when used in conjunction with different bulk elasticity laws, yield a wider family of *modified* Terzaghi compaction models. The original Terzaghi compaction model with Roscoe-Burland bulk elasticity is a particular member of this family.

Remark 4.2 *This alternative hardening model used in conjunction with linear elasticity is not a novelty itself, but the assessment of its impact on the shape of the NCL in the* v *vs.* $\log(-p_c)$ *representation seems to have been neglected in the literature. The resulting compaction curves for this hardening model used together with the proposed bulk elasticity laws will be discussed below.*

The Terzaghi compaction model. Elastoplastic description

The original Terzaghi compaction model is described by means of the NCL, which relates the normal compaction pressure, p_c, to the specific volume, v_c, as observed during a virgin compression experiment, by

$$v_c = N - \lambda \ln(-p_c), \tag{58}$$

where the constant λ is the *compression index* or *gradient of the compression line* and N (also a constant) the *specific volume intercept* at $p_c = -1$. The NCL is represented as a straight line in a v vs. $\log(-p)$ graph, as seen in Figure 3. When cast within an elastoplasticity framework in conjunction with the classical Roscoe-Burland bulk elasticity model, the Terzaghi compaction model yields a *hardening* law for the evolution of p_c – the hardening thermodynamic force in the elastoplastic context – that can be written in rate form as [15, pp 93-97]

$$\frac{\dot{p}_c}{p_c} = -\frac{v}{\lambda - \kappa}\dot{\varepsilon}_v^p, \tag{59}$$

where the rate of p_c is explicitly expressed as a function of the volumetric *plastic* strain rate. If the bulk elasticity models discussed in section 3 were to be used instead, the evolution of p_c would still be expressed in the same format as (59) but

with κ replaced with the (variable) effective swelling index κ_{eff}, i.e.

$$\frac{\dot{p}_c}{p_c} = -\frac{v}{\lambda - \kappa_{\text{eff}}}\dot{\varepsilon}_v^p, \tag{60}$$

with each bulk elasticity model having an appropriate definition of κ_{eff}. In this case, the linear bulk elasticity model has

$$\kappa_{\text{eff}} = \kappa_{\text{eff}}(p, v) \equiv \frac{K}{v\,p}, \tag{61}$$

and the stiffness-shifted nonlinear elasticity law uses definition (43).

A class of modified Terzaghi models

The elastoplastic framework proposed in this paper can incorporate any hardening model that can be expressed in the format (57). For example, the classical Terzaghi compaction model combined with the Roscoe-Burland bulk elasticity law (59) can be cast as (57) with

$$H(p_c, v) = -\frac{v}{\lambda - \kappa}p_c. \tag{62}$$

The models (60), on the other hand, cannot be expressed in this format. We also note that the denominator of the hardening evolution rule (60) becomes zero or negative for $\kappa_{\text{eff}} \geq \lambda$, which is clearly physically inconsistent. In the assessment of the present framework we will adopt a class of models, based on a modified Terzaghi compaction law, that can be expressed in the format (57) and, at the same time, avoids this potential inconsistency.

In this context, a class of modified Terzaghi models will be postulated by assuming a hardening law expressed as

$$\frac{\dot{p}_c}{p_c} = -\frac{v}{\chi}\dot{\varepsilon}_v^p, \tag{63}$$

where χ – assumed *constant* regardless of the adopted bulk elasticity model – has the physical meaning of a *hardening index*, together with any of the bulk elasticity models discussed in section 3. The above is equivalent to (57) with a hardening modulus

$$H(p_c, v) = -\frac{v}{\chi}p_c. \tag{64}$$

For this class of models, it is convenient to define the *effective compression index*,

$$\lambda_{\text{eff}} \equiv \ \chi + \kappa_{\text{eff}}. \tag{65}$$

Note that, since χ is a constant and κ_{eff} can be variable, the effective compression index is generally variable. This results in a modified version of the original Terzaghi compaction law, (58) expressed as

$$v_c = N - \lambda_{\text{eff}} \ln(-p_c), \tag{66}$$

whose normal compaction line is *generally non-linear* in its semi-log graph representation. This will be further discussed below. It should also be noted that λ_{eff} is dependent on the adopted elasticity model due to its dependance on κ_{eff}. This is at variance with the original Terzaghi compaction model.

Shape of the NCL for different elastic models

First, let us recall that the NCL describes the compaction behaviour of the material under *monotonic* hydrostatic compression. In this case, $p = p_c$ throughout the entire history of loading. Let us also recall that, for any given initial specific volume v_0, v_c in the normal compaction line depends only on the history of the *total* volumetric strain which, in turn, is the sum of the volumetric elastic and plastic strains.

For the linear elasticity model, the bulk elasticity response in rate form is defined by $(9)_1$ with constant K. The total volumetric strain in rate form, $\dot{\varepsilon}_v$, is the sum of the elastic and plastic components, $\dot{\varepsilon}_v^e$ and $\dot{\varepsilon}_v^p$, from $(9)_1$ and (63), respectively. Then, in the elastoplastic case we have

$$\dot{\varepsilon}_v = \dot{p}_c \left[\frac{1}{K} - \frac{\chi}{v\,p_c}\right]. \tag{67}$$

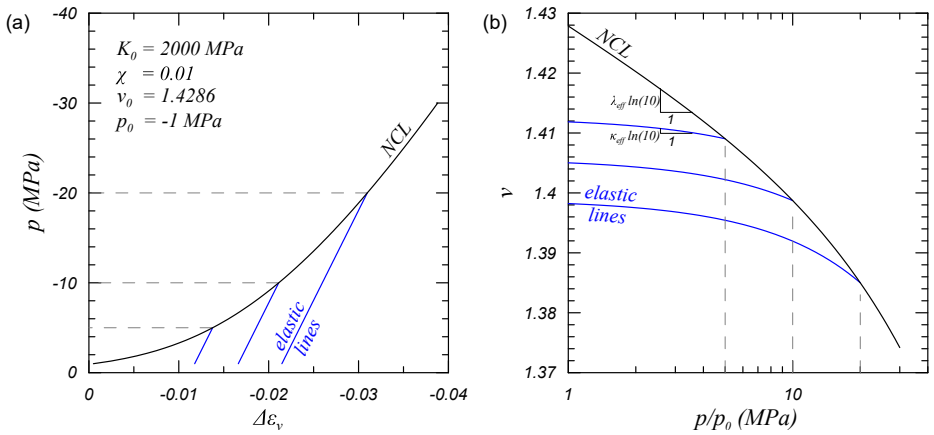

Figure 4: Shape of NCL and hydrostatic elastic (swelling) lines for the proposed hardening model in conjunction with the linear bulk elasticity model. (a) p vs. $\Delta\varepsilon_v$ graph, and; (b) v vs. $\log(p/p_0)$ graph.

For the stiffness-shifted bulk elasticity model, the volumetric elastic strain rate can be obtained from (29). By adding it to the volumetric plastic strain of the proposed hardening model (63), the rate form of the total volumetric strain for the stiffness-shifted bulk elasticity law can be expressed as

$$\dot{\varepsilon}_v = \dot{p}_c \left[\frac{\kappa}{\kappa\, K_0 - v\, p_c} - \frac{\chi}{v\, p_c} \right]. \tag{68}$$

Remark 4.3 *Note that, if the elasticity stiffness-shift parameter K_0 is set to zero, expression (68) recovers the original Terzaghi hardening law with the Roscoe-Burland bulk elasticity model presented in (60).*

For each combination of elasticity bulk model with the proposed hardening law, example representations of NCLs and swelling lines are presented in Figures 4 and 5. The results for swelling lines and the NCLs for the hardening model combined with linear bulk elasticity plotted in Figure 4 were obtained with numerical integration of expressions $(9)_1$ and (67), respectively. For the combination of the hardening model with the stiffness-shifted bulk elasticity model, the swelling lines and the NCLs plotted in Figure 5 were computed by the numerical integration of (29) and (68), respectively. In all cases, the specific volume is simultaneously numerically integrated using (11). In what follows, the numerical computation of the NCLs started from the reference state $(p, v) = (-1\text{MPa}, 1.4286)$ (equivalent to a porosity of 30%). The main material parameters are presented in the figures. The swelling lines were obtained by elastic unloading from states at the NCL with preconsolidation pressures $p_c = 5$, 10 and 20 MPa.

In the graph of Figure 4(a), the linear nature of the bulk elasticity model used is reflected on the straight shape of the swelling lines. In the usual v vs. $\log(p/p_0)$ plot of Figure 4(b) both the NCL and the swelling lines are nonlinear, with increasing nonlinearity with increasing compression. This result was already expected, given the expression (61) of the effective swelling index, k_{eff}.

On the other hand, the graphs of Figure 5 show the NCL and the swelling lines to be nonlinear in all representations. Figure 5(b), however, shows a slight linear trend of both the NCL and the swelling lines under high compression. From the definitions (43) of κ_{eff} of this bulk elasticity model and (65) of λ_{eff}, indeed, it is clear that $\lim_{p\to\pm\infty} k_{\text{eff}} = \kappa$ and also $\lim_{p\to\pm\infty} \lambda_{\text{eff}} = \lambda$.

Remark 4.4 *The proposed stiffness-shifted bulk elasticity model and hardening law retrieves the original Roscoe-Burland bulk elasticity and Terzaghi hardening models, respectively, for high compression. Thus, this combination can be truly regarded as a regularisation of the original models under tension or small compression.*

Integration of the compaction model and linearisation

The numerical computations presented earlier in this section focused on obtaining the NCL, which shows the mean pressure against the *total* volumetric strain. However, the general elastoplastic framework requires the integration of the hardening law in terms of the *plastic* volumetric strain. Analogously to the semi-analytical integration of the bulk elastic law seen

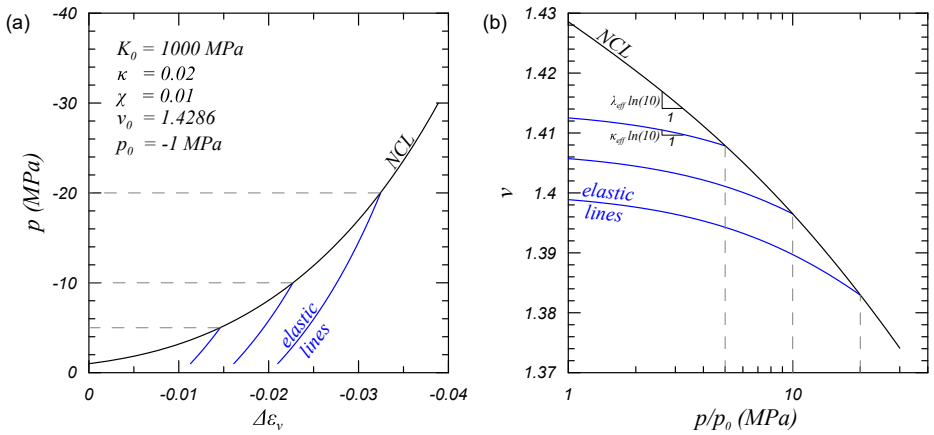

Figure 5: Shape of NCL and hydrostatic elastic (swelling) lines for the proposed hardening model in conjunction with the stiffness-shifted bulk elasticity model. (a) p vs. $\Delta\varepsilon_v$ plot, and; (b) v vs. $\log(p/p_0)$ plot.

in section 3, the integration of the hardening law (63), of the class of modified Terzaghi models considered in the present framework, between pseudo-times t_n and t_{n+1} can be approximated by holding the specific volume v constant equal to $\bar{v}$ during the step. This gives

$$p_c \simeq p_c(\Delta\varepsilon_v^p, \Delta\varepsilon_v) = p_{cn} e^{-\frac{\bar{v}}{\chi}\Delta\varepsilon_v^p}, \tag{69}$$

where the dependence of p_c on $\Delta\varepsilon_v$ comes from the numerical integration rule (33, 34). Note that when $\theta = 0$ there is no such dependence.

Remark 4.5 *The semi-analytical integration scheme with $\theta = 0$ is widely adopted in the integration of the Terzaghi compaction law [12, 34]. This semi-analytical integration approach has been applied more often in the hardening law than in the bulk elastic modulus. This points to a curious asymmetry in the implementations of many authors, like Anadarajah [12], where the hardening law is integrated as above but the bulk elasticity law is integrated by a pure Euler scheme.*

Expression (69) has the same format as the integration of the Roscoe-Burland bulk elasticity constitutive model (32). Thus, the same benefits identified in the accuracy assessment results of section 3.2 apply here.

Remark 4.6 *In the present work, the semi-analytical approach is adopted for both the hardening and bulk elasticity laws, with $\theta = 0$ and $\theta = 1$ alternatives. The latter is adopted in the novel fully-implicit Euler integration proposed in this paper.*

Within the present framework, the linearisation of (69) will be required to assemble the constitutive tangent operator consistent with the adopted integration scheme. Its linearised version reads:

$$dp_c = h^p \, d\varepsilon_v^p + h^t \, d\varepsilon_v, \tag{70}$$

with $h^p \equiv \partial p_c/\partial\varepsilon_v^p$ and $h^t \equiv \partial p_c/\partial\varepsilon_v$ the hardening moduli due to plastic and total volumetric strain. For the compaction hardening model presented in this section,

$$h^p(\Delta\varepsilon_v^p, \Delta\varepsilon_v) = -\frac{\bar{v}}{\chi} p_c(\Delta\varepsilon_v^p, \Delta\varepsilon_v) \tag{71}$$

and

$$h^t(\Delta\varepsilon_v^p, \Delta\varepsilon_v) \equiv \frac{dp_c}{d\bar{v}} \frac{d\bar{v}}{d\Delta\varepsilon_v} = \begin{cases} 0 & \text{for } \theta = 0 \\ \Delta\varepsilon_v^p \, h^p(\Delta\varepsilon_v^p, \Delta\varepsilon_v) & \text{for } \theta = 1. \end{cases} \tag{72}$$

It is particularly convenient for the solution of the return mapping equations in the present context that we expand the scalar relation above in terms of the strain invariants (6):

$$dp_c = \vec{H}^t \cdot d\Delta\vec{\varepsilon} + \vec{H}^p \cdot d\Delta\vec{\varepsilon}^p; \tag{73}$$

where $\vec{H}^p$ and $\vec{H}^p$ are coefficient vectors representing the gradients of p_c with respect to the plastic and total strain invariants:

$$\vec{H}^p = \begin{bmatrix} h^p(\Delta\varepsilon_v^p, \Delta\varepsilon_v) \\ 0 \end{bmatrix}; \qquad \vec{H}^t = \begin{bmatrix} h^t(\Delta\varepsilon_v^p, \Delta\varepsilon_v) \\ 0 \end{bmatrix}. \tag{74}$$

5 The elastoplastic constitutive problem

The generalised elastoplastic constitutive problem considers a given discrete strain increment $\Delta\boldsymbol{\varepsilon}^*$ imposed over a pseudo-time step $[t_n, t_{n+1}]$. The internal state variables – taken here as the plastic strain, $\boldsymbol{\varepsilon}^p$, and the hardening variable, α – are known at t_n. In the proposed elastoplastic framework, the hardening variable is the plastic volumetric strain itself, ε_v^p. With (7), (14) and $(20)_1$, the discretised backward Euler version of the elastoplastic constitutive initial value problem consists in finding the unknowns $\boldsymbol{\varepsilon}^e$ and ε_v^p at t_{n+1} and $\Delta\gamma$ such that

$$\begin{cases} \boldsymbol{\varepsilon}^e_{n+1} = \boldsymbol{\varepsilon}^e_n + \Delta\boldsymbol{\varepsilon}^* - \Delta\gamma \boldsymbol{N}_{n+1} \\ \varepsilon^p_{vn+1} = \varepsilon^p_{vn} + \Delta\gamma N_{vn+1} \end{cases}, \tag{75}$$

where $\boldsymbol{N}_{n+1} \equiv \boldsymbol{N}(\vec{\sigma}_{n+1}, p_{c_{n+1}})$ and $N_{vn+1} \equiv \mathrm{tr}(\boldsymbol{N}_{n+1})$. The time stage subscripts at t_{n+1} are shown in this section for clarity. The system of equations (75) is subject to the complementarity conditions enforced at t_{n+1}:

$$\Phi(\boldsymbol{\sigma}_{n+1}, p_{c_{n+1}}) \leq 0, \qquad \Delta\gamma \geq 0 \qquad \Delta\gamma\, \Phi(\boldsymbol{\sigma}_{n+1}, p_{c_{n+1}}) = 0, \tag{76}$$

with $\boldsymbol{\sigma}$ and p_c obtained by numerical integration as described in sections 3 and 4.

The above set of equations lead to a classical elastic predictor/plastic corrector algorithm [9, 11, 12] consisting of:

- An *elastic predictor* or *elastic trial* stage, where the strain increment is supposed to be purely elastic. Hence, $\Delta\gamma \equiv 0$ and only $(76)_1$ remains unchecked. The trial state at t_{n+1} (indicated with subscript tr) obtained from (75), is defined by

  $$\boldsymbol{\varepsilon}^e_{tr} \equiv \boldsymbol{\varepsilon}^e_n + \Delta\boldsymbol{\varepsilon}^*, \qquad \varepsilon^p_{vtr} \equiv \varepsilon^p_{vn}, \tag{77}$$

  and the corresponding integrated $\boldsymbol{\sigma}_{tr}$ and $p_{c_{tr}} = p_{c_n}$. If $\Phi(\boldsymbol{\sigma}_{tr}, p_{c_{tr}}) \leq 0$, the elastic trial state is consistent with the discrete complementarity rule and is accepted as the integrated solution:

  $$\boldsymbol{\varepsilon}^e_{n+1} := \boldsymbol{\varepsilon}^e_{tr}; \qquad \varepsilon^p_{vn+1} := \varepsilon^p_{vtr}; \qquad \boldsymbol{\sigma}^e_{n+1} := \boldsymbol{\sigma}^e_{tr}; \qquad p_{c_{n+1}} := p_{c_{tr}}. \tag{78}$$

  If $\Phi(\boldsymbol{\sigma}_{tr}, p_{c_{tr}}) > 0$, then the trial state violates the complementarity rule and the plastic corrector is executed;

- A *plastic corrector* or *return mapping algorithm*, where (75) is solved together with the plastic consistency condition

  $$\Phi(\boldsymbol{\sigma}_{n+1}, p_{c_{n+1}}) = 0, \tag{79}$$

  with $\Delta\gamma > 0$.

5.1 The return mapping in the two-invariant space

The return mapping can be expressed in the two-invariant space under the conditions to be presented below. This produces a return mapping that is radial in the deviatoric space, which is a fundamental part of the proposed elastoplastic framework. In this sense, it is convenient to write the deviatoric tensor component of $(75)_1$ using the discretized version of $(20)_2$:

$$\Delta\boldsymbol{\epsilon}^e = \Delta\boldsymbol{\epsilon} - \Delta\gamma \boldsymbol{N}_{\boldsymbol{\epsilon}n+1}. \tag{80}$$

Applying the secant shear elastic relation $(45)_2$ to the deviatoric strain increment above and recalling $\boldsymbol{s}_{n+1} = \boldsymbol{s}_n + \Delta\boldsymbol{s}$ together with $(18)_2$, the deviatoric stress update becomes

$$\boldsymbol{s}_{n+1} = \boldsymbol{s}_{tr} - \sqrt{6}\bar{G}\Delta\gamma \left[\frac{\partial\Psi}{\partial q}\right]_{n+1} \frac{\boldsymbol{s}_{n+1}}{\|\boldsymbol{s}_{n+1}\|}. \tag{81}$$

where $\bar{G}$ is the appropriate shear modulus and $\boldsymbol{s}_{tr}$ the trial deviatoric stress, defined by

$$\boldsymbol{s}_{tr} \equiv \boldsymbol{s}_n + 2\bar{G}\Delta\boldsymbol{\epsilon}. \tag{82}$$

In expression (81), $\boldsymbol{s}_{n+1}$ and $\boldsymbol{s}_{tr}$ are found to be *collinear*, with

$$\hat{\boldsymbol{n}} \equiv \frac{\boldsymbol{s}_{n+1}}{\|\boldsymbol{s}_{n+1}\|} = \frac{\boldsymbol{s}_{tr}}{\|\boldsymbol{s}_{tr}\|}. \tag{83}$$

Remark 5.1 *Note that the collinearity of $\boldsymbol{s}_{n+1}$ and $\boldsymbol{s}_{tr}$ is intrinsically related to the choice of a backward Euler as the integration scheme in (80).*

This collinearity allows expression (81) to be reduced to a scalar shear stress update equation with $(1)_2$:

$$q_{n+1} = q_{tr} - 3\bar{G}\Delta\varepsilon_d^p, \tag{84}$$

with q_{tr} the trial von Mises stress,

$$q_{tr} \equiv \sqrt{\frac{3}{2}}\|\boldsymbol{s}_n + 2\bar{G}\Delta\boldsymbol{\epsilon}\|. \tag{85}$$

Expressions (84, 85) in conjunction with Table 1 completely define the stress update equation of the present elastoplastic framework in the two-invariant space. Further, let us recall the plastic flow vector $\vec{N} = \vec{N}(\vec{\sigma}, p_c)$ and its invariant components (17) and $(18)_1$ to build the system of equations of the return mapping:

$$\begin{cases} \Phi_{n+1} = 0 \\ \vec{\varepsilon}^{\,e}_{n+1} = \vec{\varepsilon}^{\,e}_{n} + \Delta\vec{\varepsilon} - \Delta\gamma\vec{N}_{n+1} \\ \varepsilon^p_{vn+1} = \varepsilon^p_{vn} + \Delta\gamma N_{vn+1} \end{cases}, \tag{86}$$

with $\vec{\varepsilon}^{\,e}$ the elastic strain invariants $(6)_2$ with two independent scalar components and $\Phi_{n+1} \equiv \Phi(\boldsymbol{\sigma}_{n+1}, p_{c_{n+1}})$. The system has a total of four scalar unknowns in $\vec{\varepsilon}^{\,e}$, ε_v^p and $\Delta\gamma$.

Remark 5.2 *The return mapping in the two-invariant space imposes an additional constraint on elastoplastic models paired with the INhE elasticity law in the proposed elastoplastic framework. In these particular cases, the yield function must not depend on the third invariant, i.e. we must have*

$$\partial\Phi/\partial\Theta = 0. \tag{87}$$

where Θ is the Lode angle. Recall that, at the outset, we have assumed $\partial\Psi/\partial\Theta = 0$ in (16). Hence, equations (86) of the return mapping become independent of the third invariant and the procedure can be executed in the two-invariant space. For the ILE and INE elasticity models, however, the two-invariant format remains valid even when the yield criterion depends on the third invariant because, in such cases, $\partial\Theta/\partial\vec{\varepsilon}^{\,e} = \vec{0}$ and $\partial\Theta/\partial\varepsilon_v^p = \partial\Theta/\partial\Delta\gamma = 0$.

Note that $\boldsymbol{s}_{tr}$ in (82) and q_{tr} in (85) are computed from $\boldsymbol{s}_n$, $\Delta\boldsymbol{\epsilon}$ and $\bar{G}$. In the return mapping, $\boldsymbol{s}_n$ and $\Delta\boldsymbol{\epsilon}$ are given. For the ILE and INE elasticity models proposed in section 3, $\bar{G} \equiv G$ is also a given constant and so are $\boldsymbol{s}_{tr}$, q_{tr} and $\hat{\boldsymbol{n}}$ in their respective elastoplastic models. In the INhE elasticity model, however, (47, 48) give $\bar{G} \equiv \bar{G}(\Delta\varepsilon_v^e, \Delta\varepsilon_v)$. In this case, recalling that $\Delta\varepsilon_v = \Delta\varepsilon_v^*$ is given in the return mapping, the shear trial stresses $\boldsymbol{s}_{tr}$ and q_{tr} are computed based on $\Delta\varepsilon_v^e$, which is a function of the unknown ε_v^p of the system of equations $(86)_2$ stemming from the flow rule and the hardening law. Hence, the elastoplasticity models that rely on the INhE elasticity law yield a shear trial state ($\boldsymbol{s}_{tr}$, q_{tr}) and $\hat{\boldsymbol{n}}$ that vary during the return mapping iterations, when solved by a numerical iterative solution scheme.

Remark 5.3 *For the elastoplastic problem using the INhE elasticity model, the update of the trial Mises stress (q_{tr}) in each iteration may be simplified with benefits to the computational performance of the return mapping. The INhE elasticity model in the present framework constraints the yield criterion to be computed on the two-invariant space, as outlined in the remark 5.2. In this context, $\boldsymbol{s}_{tr}$ is not required to be computed along the iterative process. Recalling that $\boldsymbol{s}_n$ and $\Delta\boldsymbol{\epsilon}$ are given, the expression (85) can be optimised by expanding the tensor norm*

$$q_{tr} = \sqrt{\frac{3}{2}\left(\|\boldsymbol{s}_n\|^2 + 4\bar{G}\,\boldsymbol{s}_n \cdot \Delta\boldsymbol{\epsilon} + 4\bar{G}^2\,\|\Delta\boldsymbol{\epsilon}\|^2\right)}, \tag{88}$$

where the scalars $\|\boldsymbol{s}_n\|^2$, $\boldsymbol{s}_n \cdot \Delta\boldsymbol{\epsilon}$ and $\|\Delta\boldsymbol{\epsilon}\|^2$ are constant during the return mapping iterations and are computed prior to the start of the iterative process. The computation of $\boldsymbol{s}_{tr}$ is only necessary when computing the final stress state at the end of the return mapping.

The derivative $^{\partial q}/_{\partial \bar{K}}$ will be required later to compute the tangent operators consistent with the elastoplastic algorithms for the INhE elasticity model. It is given by

$$\frac{\partial q}{\partial \bar{K}} = \begin{cases} 3r \left[\frac{1}{q_{tr}} \left(\boldsymbol{s}_n \cdot \Delta\boldsymbol{\epsilon} + 2\bar{G}\|\Delta\boldsymbol{\epsilon}\|^2 \right) - \Delta\varepsilon_d^p \right] & \text{for } q_{tr} > 0 \\ 0, & \text{for } q_{tr} \approx 0 \end{cases} \tag{89}$$

where the scalars $\boldsymbol{s}_n \cdot \Delta\boldsymbol{\epsilon}$ and $\|\Delta\boldsymbol{\epsilon}\|^2$ are computed prior to the start of the iterative process. Also note that expression (89) may be used in the context of pure elasticity, with $\Delta\varepsilon_d^p = 0$ and $q_{tr} = q$. It produces the derivative $^{\partial q}/_{\partial \bar{K}}$ for the INhE elasticity model, referred to in section 3.3.

5.2 Compact system of equations

The particular choice of ε_v^p as the hardening variable allows the system of equations in (86) to be reduced. By rewriting the strain update $(86)_2$ in terms of the two-invariant plastic strain components (21), equation $(86)_3$ becomes redundant and can be removed from the system. By noticing that $\Delta\varepsilon_v^p$, $\Delta\varepsilon_d^p$ and $\Delta\gamma$ are related by (21), the two-invariant plastic strain update expressions can be replaced by the enforcement of collinearity between $\Delta\vec{\varepsilon}^p$ and $\vec{N}$. The return mapping then reduces to the compact system of two equations to be solved only for the scalar unknowns $\Delta\varepsilon_v^p$ and $\Delta\varepsilon_d^p$ (or simply $\Delta\vec{\varepsilon}^p$):

$$\begin{cases} \Phi = 0 \\ \frac{1}{\|\vec{N}\|} \left(\Delta\varepsilon_v^p N_d - \Delta\varepsilon_d^p N_v \right) = 0 \end{cases} \tag{90}$$

with $\vec{N} = \vec{N}(\vec{\sigma}, p_c)$ and $\Phi = \Phi(\boldsymbol{\sigma}, p_c)$ computed at t_{n+1} (subscript $n+1$ suppressed for convenience). Note that, in $(90)_2$, the division by $\|\vec{N}\|$ makes the equation dimensionless. If Φ is also made non-dimensional, the system of equations becomes itself dimensionless, which is particularly important to preserve objective convergence tolerances.

The expression (90) is the fundamental system of equations of the return mapping of the elastoplastic framework proposed here. Note that for any given $\Delta\vec{\varepsilon}^p$, the corresponding $\boldsymbol{\sigma}$ and p_c can be trivially computed by means of numerical integration, as described in sections 3 and 4 and – given the radial return mapping in the deviatoric space – with $\Theta = \Theta_{tr}$. In the particular case of the presented elasticity laws, $\boldsymbol{\sigma}$ is given by the expressions of Table 1 together with (84, 85) and, for the family of modified Terzaghi compaction laws, p_c is given by means of expression (69).

Remark 5.4 *This system (90) is inherently compact, with only two unknowns. This is in contrast the traditional approach [33, 34, 35] where the return mapping algorithms typically comprise systems of four equations.*

This formulation may be regarded as a return mapping in the strain invariant space alternative to that proposed by Borja and Tamagnini [36]. These authors presented a compact return mapping with a three-equation system that could be further reduced to two equations by static condensation. However, they aimed at finite strain and restricted their formulation to conservative elasticity models. Their formulation also involves an intermediate projection onto the principal stretch space, which is not needed here. These two aspects make the new proposed formulation more attractive in terms of supported elasticity models and required computational effort.

The complementarity loading/unloading condition $(76)_2$ still requires the elastoplastic problem solution to observe $\Delta\gamma > 0$. The value of $\Delta\gamma$ can be obtained through the projection

$$\Delta\gamma = \frac{\Delta\vec{\varepsilon}^p \cdot \vec{N}}{\|\vec{N}\|^2}. \tag{91}$$

Alternatively, as the complementarity condition imposes restrictions on the sign of $\Delta\gamma$ only, the following simpler check suffices:

$$\Delta\vec{\varepsilon}^p \cdot \vec{N} > 0. \tag{92}$$

5.3 Residual linearisation

Let us define the return mapping residual vector,

$$\vec{r}(\Delta\vec{\varepsilon}^p, \Delta\vec{\varepsilon}) \equiv \begin{bmatrix} \Phi \\ \frac{1}{\|\vec{N}\|} \left(\Delta\varepsilon_v^p N_d - \Delta\varepsilon_d^p N_v \right) \end{bmatrix}. \tag{93}$$

The residual is written in terms of the plastic and total strain increments. The linearisation of $\vec{r}$ is obtained by recalling the strain split (7), the two-invariant form of the flow rule (21) and the linearised versions of the elasticity (50) and hardening (73) models:

$$d\vec{r} = \tilde{L}\, d\Delta\vec{\varepsilon} + \tilde{J}\, d\Delta\vec{\varepsilon}^{\,p}; \tag{94}$$

where

$$\tilde{L} \equiv \frac{\partial \vec{r}}{\partial \Delta\vec{\varepsilon}} = \tilde{M}_\sigma \left(\tilde{C}^t + \tilde{C}^e\right) + \vec{V} \otimes \vec{H}^t; \tag{95}$$

$$\tilde{J} \equiv \frac{\partial \vec{r}}{\partial \Delta\vec{\varepsilon}^{\,p}} = \tilde{M}_{\varepsilon^p} - \tilde{M}_\sigma \tilde{C}^e + \vec{V} \otimes \vec{H}^p. \tag{96}$$

with the linearised matrix and vector operators $\tilde{M}_{\varepsilon^p} \equiv \frac{\partial \vec{r}}{\partial \Delta \vec{\varepsilon}^{\,p}}$, $\tilde{M}_\sigma \equiv \frac{\partial \vec{r}}{\partial \vec{\sigma}}$ and $\vec{V} \equiv \frac{\partial \vec{r}}{\partial p_c}$ dependant on the yield function and on the flow rule through the relations

$$\tilde{M}_{\varepsilon^p} = \frac{1}{\|\vec{N}\|} \begin{bmatrix} 0 & 0 \\ N_d & -N_v \end{bmatrix}; \qquad \tilde{M}_\sigma = \begin{bmatrix} \left[\frac{\partial \Phi}{\partial \vec{\sigma}}\right]^T \\ \left(\vec{V}_N\right)^T \frac{\partial \vec{N}}{\partial \vec{\sigma}} \end{bmatrix}; \qquad \vec{V} = \begin{bmatrix} \frac{\partial \Phi}{\partial p_c} \\ \vec{V}_N \cdot \frac{\partial \vec{N}}{\partial p_c} \end{bmatrix}, \tag{97}$$

with

$$\vec{V}_N \equiv \frac{\partial r_2}{\partial \vec{N}} = \frac{1}{\|\vec{N}\|} \left\{ \begin{bmatrix} -\Delta\varepsilon_d^p \\ \Delta\varepsilon_v^p \end{bmatrix} - \frac{\vec{N}}{\|\vec{N}\|} r_2 \right\}, \tag{98}$$

where r_2 is the second component of the residual $\vec{r}$. The system Jacobian is defined in (95) and (96) and is modular, which allows the construction of linearised systems of equations for any constitutive models compliant with the assumptions of the present framework.

5.4 Solution and tangent operator

Since the total strain increment $\Delta\vec{\varepsilon}^*$ is fixed in the return mapping, $\tilde{L} = \tilde{0}$ throughout the iterations. The residual has $\Delta\vec{\varepsilon}^p$ as the only unknown and $\tilde{J}$ becomes the Jacobian. The system of equations can be solved by a conventional Newton-Raphson scheme. At the converged solution, condition (92) must hold.

At the converged return mapping solution, the strain split together with the Taylor expansion of $\vec{r}$ around $(\Delta\vec{\varepsilon}^*, \Delta\vec{\varepsilon}^p)$, we obtain

$$\tilde{T} \equiv \frac{d\vec{\varepsilon}^e}{d\vec{\varepsilon}} = \tilde{I} - \tilde{J}^{-1}\, \tilde{L}. \tag{99}$$

Given the relation (99) and the linearisation (50) of the elastic stiffness operator, the elastoplastic constitutive tangent consistent with the algorithm in the two-invariant space, defined as

$$\tilde{D}^{ep} \equiv \frac{\partial \vec{\sigma}}{\partial \vec{\varepsilon}} = \begin{bmatrix} \frac{\partial p}{\partial \varepsilon_v} & \frac{\partial p}{\partial \varepsilon_d} \\ \frac{\partial q}{\partial \varepsilon_v} & \frac{\partial q}{\partial \varepsilon_d} \end{bmatrix}, \tag{100}$$

can be expressed as

$$\tilde{D}^{ep} = \tilde{C}^e\, \tilde{T} + \tilde{C}^t, \tag{101}$$

noting that all quantities involved in the computation of the tangent operator are values at their converged solution. In the case of a purely elastic increment, the elastoplastic tangent (101) retrieves the elastic tangent, $\tilde{C} = \tilde{C}^e + \tilde{C}^t$, in the two-invariant space.

The computation of $\tilde{D}^{ep}$ requires the inversion of a 2×2 matrix in (99), which is much less expensive than the inversion of a 4×4 system as proposed in general elastoplastic solvers [11].

5.5 Tensor form

Once the solution ($\Delta\varepsilon_v^p$, $\Delta\varepsilon_d^p$) (or simply $\Delta\vec{\varepsilon}^p$) of the above return mapping is obtained in terms of the two-invariant representation, the plastic strain tensor is updated trivially by using the spherical-deviatoric decomposition (18, 20) as

$$\boldsymbol{\varepsilon}^p = \boldsymbol{\varepsilon}_n^p + \frac{1}{3}\Delta\varepsilon_v^p\,\boldsymbol{I} + \sqrt{\frac{3}{2}}\Delta\varepsilon_d^p\,\hat{\boldsymbol{n}}. \tag{102}$$

Similarly, from (1, 2) and the values of p, q and $\hat{\boldsymbol{n}}$ at the solution,

$$\boldsymbol{\sigma} = p\,\boldsymbol{I} + \sqrt{\frac{2}{3}}q\,\hat{\boldsymbol{n}}. \tag{103}$$

The expression for the fourth-order elastoplastic consistent tangent tensor,

$$\mathbb{D}^{ep} \equiv \frac{\partial\boldsymbol{\sigma}}{\partial\boldsymbol{\varepsilon}}, \tag{104}$$

follows by taking derivatives of (103), as an extension to the development of Borja *et al.* [35]:

$$\begin{aligned}
\mathbb{D}^{ep} = &\left(\tilde{D}_{11} - \frac{1}{3}g\right)\boldsymbol{I}\otimes\boldsymbol{I} \;+\; g\,\mathbb{I}_s + \\
&+ \left[\frac{2}{3}\tilde{D}_{22} - g - \sqrt{\frac{2}{3}}\tilde{T}_{12}\,t\,(\Delta\boldsymbol{\epsilon}\cdot\hat{\boldsymbol{n}})\right]\hat{\boldsymbol{n}}\otimes\hat{\boldsymbol{n}} + \\
&+ \sqrt{\frac{2}{3}}\tilde{D}_{12}\,\boldsymbol{I}\otimes\hat{\boldsymbol{n}} + \\
&+ \left[\sqrt{\frac{2}{3}}\tilde{D}_{21} - \tilde{T}_{11}\,t\,(\Delta\boldsymbol{\epsilon}\cdot\hat{\boldsymbol{n}})\right]\hat{\boldsymbol{n}}\otimes\boldsymbol{I} + \\
&+ \tilde{T}_{11}\,t\,\Delta\boldsymbol{\epsilon}\otimes\boldsymbol{I} + \\
&+ \sqrt{\frac{2}{3}}\tilde{T}_{12}\,t\,\Delta\boldsymbol{\epsilon}\otimes\hat{\boldsymbol{n}},
\end{aligned} \tag{105}$$

where $\mathbb{I}_s$ is the forth-order symmetric identity tensor, $\boldsymbol{I}$ the second-order identity tensor, $\cdot$ denotes the scalar product, $\otimes$ the tensor product and

$$g = 2\bar{G}\frac{q}{q_{tr}}, \tag{106}$$

and

$$t = 2\frac{d\bar{G}}{d\varepsilon_v^e}\frac{q}{q_{tr}}. \tag{107}$$

The terms with t in (105) need to be computed only if the shear modulus $\bar{G}$ is variable (INhE elastic model). If the trial stress state is hydrostatic, (105) reduces to:

$$\mathbb{D}|_{q_{tr}=0} = \left[\tilde{D}_{11} - \frac{2}{9}\tilde{D}_{22}\right]\boldsymbol{I}\otimes\boldsymbol{I} + \frac{2}{3}\tilde{D}_{22}\,\mathbb{I}_s. \tag{108}$$

5.6 Summary

This section presented the formulation of the integration framework for the modular elastoplastic constitutive problem proposed in the present paper. It also discussed the impacts of each element of the elastoplastic constitutive problem in the formulation and the compatibility constraints. The algorithms and the implementation details satisfying the conditions presented here are detailed in the Appendix A.

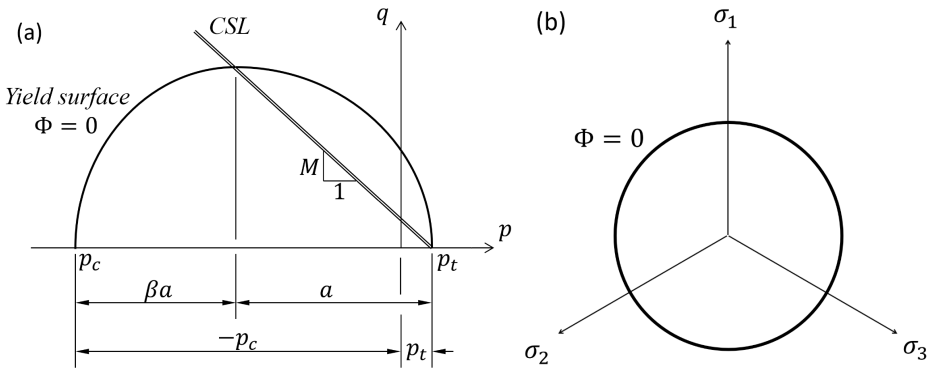

Figure 6: The adopted generalised MCC yield surface.
a) p-q plane representation; b) deviatoric plane representation.

6 Accuracy and performance

This section presents an assessment of the performance and finite-step accuracy of the proposed elastoplastic framework against existing formulations. The flexibility of the framework allows it to be compared against a range of formulations in the family of isotropic elastoplastic constitutive models. To keep it brief, the assessment will use the most common elastoplastic constitutive model adopted in the analysis of geomaterials – the *Modified Cam-Clay* model. For this model there is a very efficient elastoplastic formulation proposed by Borja [34] that will be used here as a benchmark for the comparisons. Borja postulated a return-mapping based on a system of four nonlinear equations paired with a closed-form expansion towards the tensorial stress and strain spaces for the consistent stiffness tensor. His expansion thus dismisses the typical numerical inversion of a 4x4 matrix to compute the stiffness tensor. The authors believe that, if the novel formulation is competitive to that of Borja, then it should be competitive to any other formulation in the literature.

The Modified Cam-Clay model is retrieved in the present modular framework by using the elasticity model INhE with zero stiffness-shift, $K_0 = 0$. The model is coupled with associative flow.

6.1 Yield function and flow rule. The Modified Cam-Clay

The Modified Cam-Clay (MCC) elastoplastic constitutive model as proposed by Roscoe and Burland [13] has been a standard in soil and rock analysis, especially for geomaterials complying with the critical state theory. There are variants proposed to enhance predictive capability, known as *generalised Cam-Clay* models. In regards to yield criteria, some generalisations include asymmetry in the hydrostatic semi-axes of the ellipse in the compaction and dilation zones [31, 11, 32], asymmetry on the deviatoric plane [31, 32] and tensile domain [11, 32].

The present work adopts the yield surface schematically represented in Figure 6 in the p-q and deviatoric projections. The *critical state line* (CSL) is presented in Figure 6(a) as a double line. It is the alternative documented by de Souza Neto *et al.* [11] with the normalising factor $1/a^2$ proposed by Sanei *et al.* [32]:

$$\Phi(\vec{\sigma}, p_c) = \frac{1}{b^2}\left(\frac{p - p_t}{a} + 1\right)^2 + \left(\frac{q}{Ma}\right)^2 - 1, \tag{109}$$

with p_c always negative and a and b given by

$$a(p_c) = \frac{p_t - p_c}{1 + \beta}; \qquad b = \begin{cases} 1 & p \geq p_t - a \\ \beta & p < p_t - a. \end{cases} \tag{110}$$

The model parameters are the tensile strength in the hydrostatic axis, p_t, the slope of the critical state line, M, and the asymmetry shape factor of the envelope in the dilatant and compactant zones, $0 < \beta \leq 1$. The envelope is a surface of revolution around the hydrostatic axis (Figure 6b). The tensile strength, p_t, not only expands the original MCC domain towards tension, but also shifts the CSL along the hydrostatic axis, as shown in Figure 6(a). The original MCC is retrieved when $p_t = 0$ and $\beta = 1$.

Within the proposed elastoplastic framework, the derivatives of the above generalised MCC yield function with respect to the stress invariants and to the hardening parameter p_c will be needed:

$$\frac{\partial \Phi}{\partial \vec{\sigma}} = \frac{2}{a} \begin{bmatrix} \frac{1}{b^2}\left(\frac{p-p_t}{a}+1\right) \\ \frac{q}{aM^2} \end{bmatrix}, \tag{111}$$

$$\frac{\partial \Phi}{\partial p_c} = \frac{2}{a}\frac{1}{(1+\beta)}\left[\Phi - \frac{1}{b^2}\left(\frac{p-p_t}{a}+1\right)+1\right]. \tag{112}$$

As in the original MCC model, associativity of the plastic flow is adopted here, i.e. $\vec{N} \equiv \frac{\partial \Psi}{\partial \vec{\sigma}} = \frac{\partial \Phi}{\partial \vec{\sigma}}$ and

$$\frac{\partial \vec{N}}{\partial \vec{\sigma}} = \frac{2}{a^2} \begin{bmatrix} \frac{1}{b^2} & 0 \\ 0 & \frac{1}{M^2} \end{bmatrix}; \tag{113}$$

$$\frac{\partial \vec{N}}{\partial p_c} = \frac{2}{a}\frac{1}{(1+\beta)}\left\{\vec{N} - \begin{bmatrix} \frac{1}{ab^2} \\ 0 \end{bmatrix}\right\}. \tag{114}$$

6.2 Numerical results

The MCC model in the proposed elastoplastic framework and the formulation of Borja were implemented here using the C++ programming language with minimum usage of object-orienting abstraction[4]. It resembles plain C for the implementation of the formulation of Borja, except for the support of matrices for the linear solver of the system of equations. On the other hand, the implementation of the present model required more object-oriented features because of the required matrix operations in the modular construction of the system of equations. It followed the algorithm detailed in the Appendix A.

Both models were implemented using the EIGEN package (v. 3.3.9) for the matrix containers and the linear algebra support. The matrix containers are dense of fixed size and based on static memory allocation. EIGEN relies on expression template strategies to expand operations and unroll loops on fixed-size matrices at compile-time, therefore reducing execution point indirections and improving native compiler optimisation of the executable code. EIGEN is claimed to perform as efficiently as the known libraries MKL, GOTO BLAS and ATLAS using dynamic-size matrices of up to 2000×2000 elements for a variety of matrix and matrix-vector operations [38]. Fixed-size matrices of sizes smaller than 16 – the case of the matrices used here fall in – are reported to perform even better.

The system of equations of the return mappings are different. Borja uses the expressions for p, q, p_c and Φ as the residual vector. The resulting system of four nonlinear equations is solved by a Newton-Raphson solver and the linearised system of equations are solved via the EIGEN implementation of partial pivot LU decomposition, which we found to be the best performing linear solver for the task. The residual developed here – equation (93) – yields a system of two nonlinear equations. It is also solved by a regular Newton-Raphson nonlinear solver and the related linearisations are computed by means of Cramer's rule.

Remark 6.1 *The proposed integrator requires very few indirections ("if" clauses) in the evaluation and none in the solution of the linearised system of equations. It suits well the SIMD (Single-Instruction, Multiple-Data) strategy of contemporary high-performance computation – as required in the usage of GPUs, for instance.*

The same convergence tolerance applied to these residual vectors may bias the requested solution quality and render the comparison unfair. To minimize this effect, the tests were proposed with an initial envelope in the range of $1 \sim 2$ MPa in the p and q variables, in magnitude. The tolerance was set to 10^{-8} in the Euclidean norm of the residual vectors. Initial guesses for the return mappings of both formulations were set at the trial state, with $p_0 = p_{tr}$, $q_0 = q_{tr}$, $p_{c0} = p_{ctr}$ and $\Delta\gamma_0 = \Delta\varepsilon_{d0} = \Delta\varepsilon_{v0} = 0$. The material parameters are $\kappa = 0.01$ and $\nu = 0.25$ for the elastic model and $\lambda = 0.02$ and $M = 1.2$ with initial preconsolidation of $p_c = -2\,MPa$ for the MCC. The extra coefficients of the present formulation are $\beta = 1$, $p_t = 0$, $K_0 = 0$ and $\theta = 0$ ($\bar{v} \equiv v_n$) to make the formulations equivalent. The initial stress lies on the hydrostatic axis, with $p = -1\,MPa$. The tests were run on an array of strain increments at an arbitrary distortional direction ($\boldsymbol{\Delta\epsilon}$) such that the trial stresses correspond to invariants in the range $p_{tr} \in [-10, -0.25]$ and $q_{tr} \in [0, 10]$ in $0.25\,MPa$ increments. The quality of the numerical solution is measured by the relative error norm δ defined as proposed by Borja and Tamagnini [36],

$$\delta \equiv \frac{\sqrt{(p-p^*)^2 + (q-q^*)^2 + (p_c-p_c^*)^2}}{\sqrt{(p^*)^2 + (q^*)^2 + (p_c^*)^2}}, \tag{115}$$

[4]Object oriented programming is known to produce executable codes with more instructions and execution point indirections than procedural programming, with negative impact on run-time performance [37].

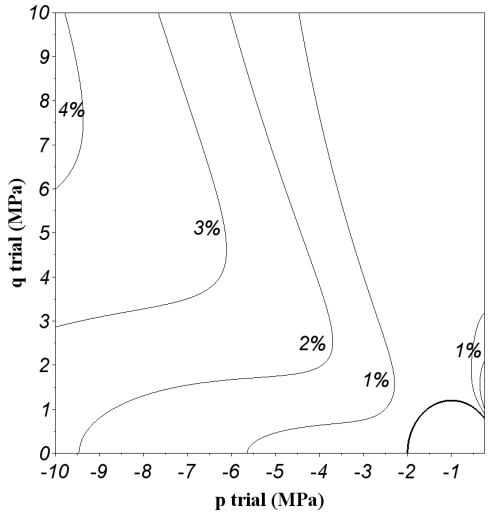

Figure 7: Isoerror map of the return mapping from each trial stress in terms of δ (115).

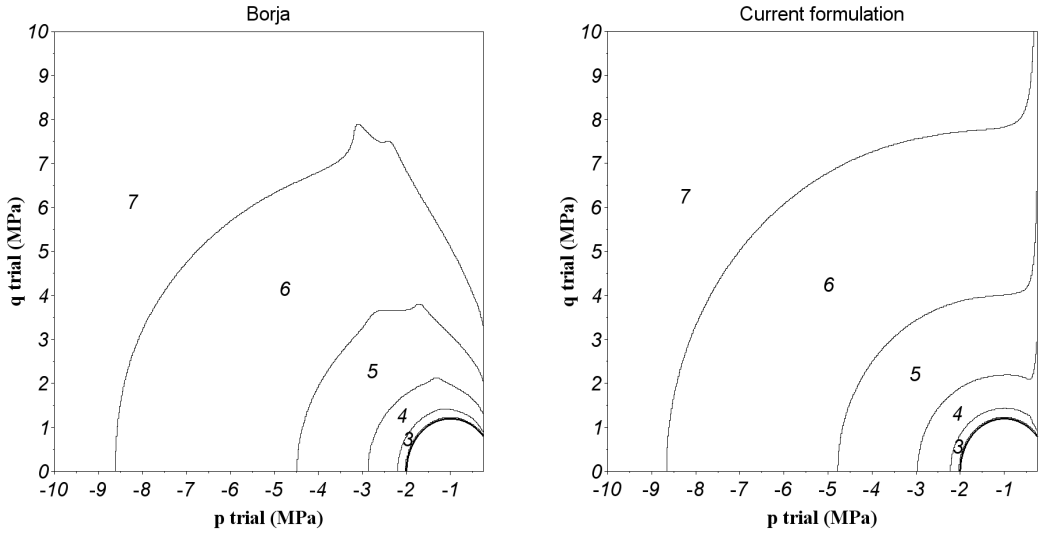

Figure 8: Return mapping. Newton-Raphson iterations.

where p^*, q^* and p_c^* are the approximations to the exact solution by applying the strain increment in sufficiently small equally-spaced substeps so as to obtain convergence of the integration algorithm within machine precision (typically around 1000 substeps were more than sufficient to achieve convergence).

Remark 6.2 *Anandarajah [12] recommends the use of solutions of explicit plasticity formulations, where available, as initial guesses in implicit solvers to improve performance. Here, the trial state was chosen instead. The authors believe that this choice should bring little to no effect on the performance ratios, as a more efficient initial guess should affect the performance of both models under comparison in the same way.*

Figure 7 presents the isoerror map in the $p - q$ plane, which is obviously valid for both formulations. The initial MCC envelope is presented in the lower-right corner, in bold line. The deviations from the "exact" solution were small in the $p_{tr} > -4\,MPa$ and $q_{tr} < 1\,MPa$ regions, with deviations of up to 2%, typically. The differences were larger in the $p_{tr} = -q_{tr}$ diagonal, with deviations of up to 4% for large trial stresses. Although these large trial stresses may appear unreasonable, especially under infinitesimal strains, it reveals the robustness of the algorithms in dealing with large strain increments.

The contours in Figure 8 indicate the number of Newton-Raphson steps each formulation required to achieve convergence within the desired tolerance. The number of required steps to solve for each trial stress is fairly similar over the

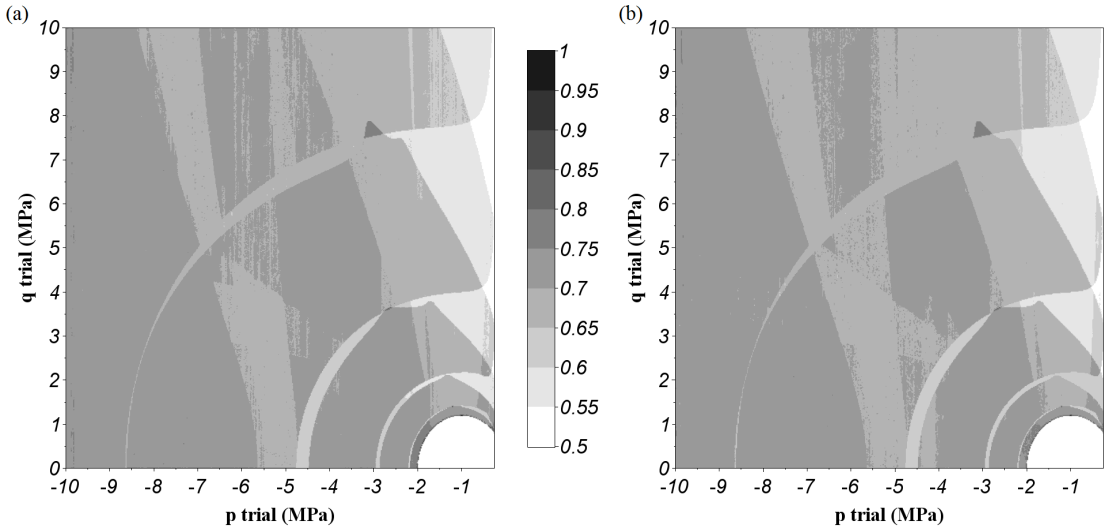

Figure 9: Ratio of the elastoplastic constitutive problem solution times of the novel formulation to the reference model of Borja [34] (a) including the computation of the updated stress and plastic strain in tensor form; and (b) also including the computation of $\mathbb{D}^{ep}$.

(p_{tr}, q_{tr}) domain, but the novel formulation requires noticeably fewer steps in the region closer to the dry side of the MCC envelope. As noticed earlier, the convergence tolerance affects each model differently given the residual variables, despite the care taken to choose appropriate testing ranges. Because quadratic convergence is expected in the Newton-Raphson algorithm near the solution, any unintended biasing in the quality of the solutions is prone to be overcome by no more than one iteration and in limited regions. The global picture is not expected to be significantly affected by any biasing.

Figure 9(a) illustrates the ratio of the clock time of the current formulation over that of Borja [34]. These tests were run[5] in a single thread over 10^5 repetitions for each trial stress. The timed execution involves the application of the strain increment in Voigt representation, the solution of the return mapping and the expansion of the stress and strain solutions to Voigt notation. In general terms, the presented procedure performs faster over the whole (p_{tr}, q_{tr}) range. It requires on average 69% of the execution time of the reference procedure. It is about 45% faster. This result is sensitive to the number of Newton-Raphson steps of each formulation and this signature is present in the gray contours. In the regions with the same number of iterations, the presented code requires 70.6% of the execution time, i.e. it is about 41% faster per iteration.

The grayscale map of Figure 9(b) includes the computation of the consistent tangent operator in Voigt notation. This execution time ratio averages to 68.8%. It indicates the performance gains in the computation of the consistent elastoplastic tangent in the proposed formulation to be of the same order as the gains observed in the return mapping solution.

7 Conclusions

An efficient modular integration framework for two-invariant-based elastoplastic constitutive models was successfully devised, which incorporates a wide family of isotropic elastoplastic models. This development was motivated by the need in the oil and gas industry for efficient geomechanical solvers and was focussed on the modelling of rock compaction in geomechanical analyses. The accurate modelling of compaction is a key element to the prediction of hydrocarbon production and potential geohazards, crucially important to decision-making in reservoir production planning and management. The elastoplastic constitutive models the framework proposed to handle are not novelties in themselves. The main contribution here is the modular environment. Within the framework, a fully-implicit scheme is obtained by setting $\theta = 1$ in the appropriate expressions of the elasticity and hardening models. This class of integrators is a novelty. Existing algorithms, popular in the literature [12, 31, 32, 33, 34], do not rely on this approach. These can be obtained here by setting $\theta = 0$. The study has also identified a number of issues in this context that appear to have been neglected in the literature.

The framework was presented with three alternative isotropic elasticity laws comprising linear and nonlinear bulk

[5]System specs: AMD Ryzen 5 4600H; Ubuntu Linux version 21.04 and gcc compiler version 11.3.

and shear elasticity models. The nonlinear bulk elasticity model is based on the well-known Roscoe-Burland swelling line of soils but implements a stiffness-shift to provide a (limited) support in the region of tensile mean stresses, which is desirable for rock modelling in the present context. This work extended the semi-analytical numerical integration proposed by Borja [34] to the stiffness-shifted bulk model and it was shown to improve numerical accuracy over the classical, pure Euler-based numerical integration. In addition, the semi-analytical integration was shown to prevent the critical issue of artificial 'volumetric locking' in the pure Euler-based integrator.

The proposed framework is capable of incorporating isotropic hardening models that take the plastic volumetric strain, ε_v^p, as the hardening variable and the preconsolidation mean stress, p_c, as the corresponding thermodynamical force. The paper discussed the Terzaghi compaction model and showed that, when used in conjunction with a bulk elasticity model other than the Roscoe-Burland law, it may lead to physical inconsistencies. The framework adopted a common alternative hardening law free from elastic terms which successfully prevented such inconsistencies. The coupling of this hardening law with different elasticity models produced a family of modified Terzaghi compaction models. Crucial insight into these models was gained by analysing and comparing their corresponding NCLs, which is needed for the determination of important model parameters from laboratory testing. These two aspects seem to have been overlooked in the literature.

The general integration algorithm was tested and compared against the formulation of Borja [34]. The model adopted by Borja can be obtained as a particular case of the class of constitutive models that can be handled by the proposed framework. Despite its modular approach, the proposed framework was found to lead to consistent significant gains in computational performance (about 45% faster). We note that such a gain in performance may be crucial to analyses in the context of the oil and gas industry, where very large scale problems are routinely solved. The performance gains can be attributed to the compact system of two equations of the general return mapping.

Acknowledgments

This work was developed during a research visit of Erick S. R. Santos to Swansea University, sponsored by Petróleo Brasileiro S.A. - Petrobras. This support is gratefully acknowledged by both authors.

References

[1] N Inoue, S. A. B. da Fontoura, G. L. Righetto, C. E. R. Lautenschlager, R. A. do C. Albuquerque, G. B. Meurer, and A. L. S de Souza. Reservoir geomechanics workflow. In *Proceedings of ISRM International Symposium - 8th Asian Rock Mechanics Symposium*, number ISRM-ARMS8-2014-194, Sapporo, Japan, 2014.

[2] Osman Hamid, Ahmed Omair, and Pablo Guizada. Reservoir geomechanics in carbonates. In Society of Petroleum Engineers, editor, *Proceedings of SPE Middle East Oil & Gas Show and Conference*, Manama, Kingdom of Bahrain, March 2017.

[3] Anthony Settari. Reservoir compaction. In *SPE Distinguished Author Series*, number SPE 76805, 2002.

[4] P.M.T.M. Schutjens, T.H. Hanssen, M.H.H. Hettema, J. Merour, P. de Bree, J.W.A. Coremans, and G. Helliesen. Compaction-induced porosity/permeability reduction in sandstone reservoirs: Data and model for elasticity-dominated deformation. In *Society of Petroleum Engineers - SPE*, number SPE 88441, 27 January 2004.

[5] Manouchehr Sanei, Omar Duran, Philippe R. B. Devloo, and Erick S. R. Santos. Evaluation of the impact of strain-dependent permeability on reservoir productivity using iterative coupled reservoir geomechanical modeling. *Journal of Petroleum Science and Engineering*, 06 2020.

[6] Luis Carlos Sousa Jr., Erick Slis Raggio Santos, and Francisco Henriques Ferreira. Geomechanical data acquisition and modeling applied to an offshore sandstone petroleum reservoir. In *Proceedings of 44th U.S. Rock Mechanics Symposium and 5th U.S.-Canada Rock Mechanics Symposium*, 2010.

[7] M. Hegazy and M. R. Lakshmikantha. Geomechanics: a new star in the horizon to change the fortunes in E&P projects. In *Proceedings of SPE Biennial Energy Resources Conference*, number SPE 169914-MS, Port of Spain, Trinidad, 09-11 June 2014.

[8] J. Simo and T. J. R. Hughes. *Computational Inelasticity*. Springer, 1998.

[9] Hai-Sui Yu. *Plasticity and Geotechnics*. Springer, 2006.

[10] W.F. Chen and D.J. Han. *Plasticity for Structural Engineers*. J. Ross Publishing Classics. J. Ross Pub., 2007.

[11] E.A. de Souza Neto, D. Perić, and D.R.J. Owen. *Computational Methods for Plasticity: Theory and Applications*. Wiley, 2008.

[12] A. Anandarajah. *Computational Methods in Elasticity and Plasticity: Solids and Porous Media*. Springer, 2010.

[13] K.H. Roscoe and John Burland. On the generalized stress-strain behavior of wet clays. 01 1968.

[14] A. Schofield and P. Wroth. *Critical State Soil Mechanics*. European civil engineering series. McGraw-Hill, 1968.

[15] D.M. Wood. *Soil Behaviour and Critical State Soil Mechanics*. Cambridge University Press, 1990.

[16] M.K. Kim and Poul Lade. Single hardening constitutive model for frictional materials I. Plastic potential function. *Computers and Geotechnics*, 5:307–324, 12 1988.

[17] Poul Lade and M.K. Kim. Single hardening constitutive model for frictional materials II. Yield criterion and plastic work contours. *Computers and Geotechnics*, 6:13–29, 12 1988.

[18] Poul Lade and M.K. Kim. Single hardening constitutive model for frictional materials III. Comparisons with experimental data. *Computers and Geotechnics*, 6:31–47, 12 1988.

[19] Poul Lade and Moon Kim. Single hardening constitutive model for soil, rock and concrete. *International Journal of Solids and Structures*, 32:1963–1978, 07 1995.

[20] Hajime Matsuoka and Teruo Nakai. Stress deformation and strength characteristics of soil under three different principal stresses. *Proceedings of the Japan Society of Civil Engineers*, 1974, 12 1974.

[21] Giuseppe Mortara. A new yield and failure criterion for geomaterials. *Geotechnique*, 58:125–132, 03 2008.

[22] A. Crook, Stephen Willson, Jianguo yu, and D.R.J. Owen. Predictive modelling of structure evolution in sandbox experiments. *Journal of Structural Geology*, 28:729–744, 05 2006.

[23] Joshua Obradors Prats, M. Rouainia, Andrew Aplin, and A. Crook. Stress and pore pressure histories in complex tectonic settings predicted with coupled geomechanical-fluid flow models. *Marine and Petroleum Geology*, 76, 04 2016.

[24] Evert Hoek and Edwin T. Brown. *Underground Excavation in Rock*. 1980.

[25] Frank L. DiMaggio and Ivan S. Sandler. Material model for granular soils. *Journal of the Engineering Mechanics Division*, 1971.

[26] Ivan S. Sandler, Frank L. DiMaggio, and George Y. Baladi. Generalized cap model for geological materials. *Journal of the Geotechnical Engineering Division*, 1976.

[27] A. Settari and Dale A. Walters. Advances in coupled geomechanical and reservoir modeling with applications to reservoir compaction. In *Proceedings of SPE Reservoir Simulations Symposium*, March 2001.

[28] Marte Gutierrez and Randall Hickman. Constitutive modeling of chalk time-dependent behavior and chalk-water interaction. pages 269–284, 08 2006.

[29] Herbert F. Wang. *Theory of Linear Poroelasticity with Applications to Geomechanics and Hydrogeology*. Princeton University Press, 2000.

[30] O. Coussy. *Poromechanics*. Wiley, 2004.

[31] Daichao Sheng, Scott Sloan, and H. Yu. Aspects of finite element implementation of critical state models. *Computational Mechanics*, 26:185–196, 08 2000.

[32] Manouchehr Sanei, Omar Duran, Philippe R. B Devloo, and Erick S. R. Santos. An innovative procedure to improve integration algorithm for modified Cam-Clay plasticity model. *Computers and Geotechnics*, 124, 05 2020.

[33] Ronaldo Borja and Seung Lee. Cam-Clay plasticity, Part I: Implicit integration of elasto-plastic constitutive relations. *Computer Methods in Applied Mechanics and Engineering*, 78:49–72, 01 1990.

[34] Ronaldo Borja. Cam-Clay plasticity, Part II: Implicit integration of constitutive equation based on a nonlinear elastic stress predictor. *Computer Methods in Applied Mechanics and Engineering*, 88:225–240, 07 1991.

[35] Ronaldo Borja, Qing Yin, and Yang Zhao. Cam-Clay plasticity. Part IX: On the anisotropy, heterogeneity, and viscoplasticity of shale. *Computer Methods in Applied Mechanics and Engineering*, 360:112695, 11 2019.

[36] Ronaldo Borja and Claudio Tamagnini. Cam-Clay plasticity. Part III: Extension of the infinitesimal model to include finite strains. *Computer Methods in Applied Mechanics and Engineering*, 155:73–95, 03 1998.

[37] Brad Calder, Dirk Grunwald, and Benjamin Zorn. Quantifying behavioral differences between C and C++ programs. *Journal of Programming Languages*, 2, 02 1994.

[38] Eigen C++ template library for linear algebra. Accessed Feb. 23, 2022 [Online].

Appendix A Algorithm for the elastoplastic constitutive problem

This Appendix summarizes the algorithm of the integration framework for the modular elastoplastic constitutive problem proposed in the present paper

The algorithm of box 1 is the entry-point for the solution of the constitutive problem. It details the execution of the elastic predictor and, if needed, the call to the plastic corrector algorithm. In the sequence, it computes the integrated state variables and the tangent operator consistent to the elastoplastic constitutive problem. The inputs to the algorithm are the material parameters, a known material state $(v, \boldsymbol{\sigma}, \boldsymbol{\varepsilon}^p, p_c)$ and the strain increment request, $\Delta\boldsymbol{\varepsilon}^*$. For clarity, the algorithm for the plastic corrector in the two-invariant space is depicted in the algorithm box 2.

One of the crucial elements of the elastoplastic constitutive problem is the elasticity law. As discussed in the paper, the choice of the elasticity law may imply additional constraints to the formulation and these require individualized execution steps. The authors chose to present an unified algorithm and to branch the specialized steps where strictly necessary. In the algorithm, this branching is presented in tabular format, with each column representing an elasticity law. Another crucial element is the dependence of the yield criterion on the third invariant. In the algorithm, the statement $\Phi = \Phi(\vec{\sigma}, p_c)$ is *true* if the yield criterion can be written as a function of the two-invariant space only. If the yield criterion depends on the third invariant, that statement evaluates to *false*. These conditions are related to the choice of elasticity model and yield criterion and are constant for a given elastoplastic constitutive model. Hence, they can be reasoned a-priori to minimise execution-time overhead. Aside from these conditions, alternative yield criteria, flow rules and hardening laws supported by the framework have no impact on the implementation stencil and are therefore transparent to the algorithm.

Remark A.1 *The computation of the updated stress in the case the yield criterion depends on the third invariant (see algorithm of box 2) can be singnificantly simplified if the yield criterion is expressed explicitly in terms of the invariants,* $\Phi = \Phi\left(\left(\vec{\sigma}, \Theta_{tr}\right), p_c\right)$. *We recall that this case does not support the elasticity model INhE. In what follows, neither* $\boldsymbol{s}_{tr}$, $\hat{\boldsymbol{n}}$ *nor* $\boldsymbol{\sigma}$ *need to be computed – the trial Lode Angle* Θ_{tr} *is computed instead. In this context,* Θ_{tr} *is constant during the iterative process.*

For brevity, the algorithm omits the determination of the tangent operator when the elastic predictor succeeds. The computation of the tangent operator is straightforward for the ILE and INE models. In the ILE case it is even constant and it can be computed outside the scope of the elastoplastic constitutive problem for optimised reuse. For the INhE model, the stiffness matrix may be obtained by applying the expansion of the elastoplastic tangent tensor of subsection 5.5 to the two-invariant form of the elasticity tangent operator, $\tilde{C}^e + \tilde{C}^t$.

We recall that not all combination of elasticity model and yield criterion type is supported in the framework, as explicitly indicated by the the assertion clause in the algorithm 2. We also note that the algorithms do not include execution exceptions nor error handling.

Algorithm 1 Solver of the elastoplastic constitutive problem

1: Elastic predictor (imposed $\Delta\boldsymbol{\varepsilon}^*$)

$\Delta\varepsilon_v^* \leftarrow tr(\Delta\boldsymbol{\varepsilon}^*)$ $\quad$ $\Delta\boldsymbol{\epsilon}^* \leftarrow \Delta\boldsymbol{\varepsilon}^* - \frac{1}{3}\Delta\varepsilon_v^*\,\boldsymbol{I}$

$\Delta\varepsilon_v^e \leftarrow \Delta\varepsilon_v^*$

$\boldsymbol{\varepsilon}_{tr}^p \leftarrow \boldsymbol{\varepsilon}_n^p$ $\quad$ $p_{ctr} \leftarrow p_{cn}$;

Compute trial stress state according to elasticity model:

ILE	INE	INhE
		$\bar{K}\,(\Delta\varepsilon_v^e, \Delta\varepsilon_v^*)$ via (48)
$p_{tr} \leftarrow p_n + K\Delta\varepsilon_v^*$	$p_{tr} \leftarrow p\,(\Delta\varepsilon_v^e, \Delta\varepsilon_v^*)$ via (35)	$p_{tr} \leftarrow p_n + \bar{K}\Delta\varepsilon_v^*$
$\boldsymbol{s}_{tr} \leftarrow \boldsymbol{s}_n + 2G\Delta\boldsymbol{\epsilon}^*$	$\boldsymbol{s}_{tr} \leftarrow \boldsymbol{s}_n + 2G\Delta\boldsymbol{\epsilon}^*$	$\boldsymbol{s}_{tr} \leftarrow \boldsymbol{s}_n + 2r\bar{K}\Delta\boldsymbol{\epsilon}^*$

$\boldsymbol{\sigma}_{tr} \leftarrow p_{tr}\,\boldsymbol{I} + \boldsymbol{s}_{tr}$

2: Check elastic admissibility

IF $\Phi(\boldsymbol{\sigma}_{tr}, p_{ctr}) \leq 0$ THEN SET $(\bullet)_{n+1} \leftarrow (\bullet)_{tr}$; $v \leftarrow v_n e^{\Delta\varepsilon_v}$ and EXIT.

3: Return mapping. Solve the system of equations

GOTO Algorithm 2;

4: Update the state variables, v, $\boldsymbol{\varepsilon}^p$, $\boldsymbol{\sigma}$ and p_c:

$v \leftarrow v_n e^{\Delta\varepsilon_v}$

Retrieve computed $\{p, q, q_{tr}, p_c, \Delta\vec{\varepsilon}^p\}$ from last iteration of the return mapping solver.

IF $q_{tr} \approx 0$ THEN

$\boldsymbol{\varepsilon}^p \leftarrow \boldsymbol{\varepsilon}_n^p + \frac{1}{3}\Delta\varepsilon_v^p\,\boldsymbol{I}$

$\boldsymbol{\sigma} \leftarrow p\,\boldsymbol{I}$

ELSE

Update the trial stress according to elasticity model:

ILE	INE	INhE
not necessary	not necessary	$\boldsymbol{s}_{tr} \leftarrow \boldsymbol{s}_n + 2r\bar{K}\Delta\boldsymbol{\epsilon}^*$

$\hat{\boldsymbol{n}} \leftarrow \frac{\boldsymbol{s}_{tr}}{\|\boldsymbol{s}_{tr}\|}$

$\boldsymbol{\varepsilon}^p \leftarrow \boldsymbol{\varepsilon}_n^p + \frac{1}{3}\Delta\varepsilon_v^p\,\boldsymbol{I} + \sqrt{\frac{3}{2}}\Delta\varepsilon_d^p\,\hat{\boldsymbol{n}}$

$\boldsymbol{\sigma} \leftarrow p\,\boldsymbol{I} + \sqrt{\frac{2}{3}}q\,\hat{\boldsymbol{n}}$

5: Compute the consistent tangent operator, if requested:

Retrieve computed $\left\{\tilde{M}_\sigma, \tilde{C}^e, \vec{V}, \tilde{J}\right\}$ from last iteration of the return mapping solver;

Compute:

ILE	INE	INhE
$\tilde{C}^t$ from $(52)_2$	$\tilde{C}^t$ from $(53)_2$	$\tilde{C}^t$ from $(54)_2$

$\vec{H}^t$ from $(74)_2$, using (72) for the case of modified Terzaghi hardening;

$\tilde{L}$, $\tilde{T}$ and $\tilde{D}^{ep}$ from (95), (99) and (101), respectively;

Compute the elastoplastic consistent tangent tensor $\mathbb{D}^{ep}$:

IF $q_{tr} \approx 0$ THEN use (108)

ELSE use (105, 106, 107)

6: EXIT

Algorithm 2 Newton-Raphson algorithm for the solution of the return mapping

1: Initialize iteration counter and propose initial guess

$i \leftarrow 0$

$\Delta\vec{\varepsilon}^p \leftarrow \vec{0}$

Prepare the following constants according to the elasticity model:

ILE	INE	INhE
		$\|\boldsymbol{s}_n\|^2$, $\boldsymbol{s}_n \cdot \Delta\boldsymbol{\epsilon}$ and $\|\Delta\boldsymbol{\epsilon}\|^2$
q_{tr} by (85)	q_{tr} by (85)	
$\tilde{C}^e$ from $(52)_1$		

IF not ($\Phi = \Phi(\vec{\sigma}, p_c)$) and $q_{tr} \neq 0$ THEN compute $\hat{\boldsymbol{n}} \leftarrow \frac{\boldsymbol{s}_{tr}}{\|\boldsymbol{s}_{tr}\|}$

2: Perform Newton-Raphson iteration

Update the stress state and the two-invariant stiffness according to the elasticity model:

ILE	INE	INhE
		$\bar{K}\left(\Delta\varepsilon_v^* - \Delta\varepsilon_v^p, \Delta\varepsilon_v^*\right)$ via (48)
		q_{tr} via (88)
$p \leftarrow p_n + K\left(\Delta\varepsilon_v^* - \Delta\varepsilon_v^p\right)$	$p\left(\Delta\varepsilon_v^* - \Delta\varepsilon_v^p, \Delta\varepsilon_v^*\right)$ via (35)	$p \leftarrow p_n + \bar{K}\left(\Delta\varepsilon_v^* - \Delta\varepsilon_v^p\right)$
$q \leftarrow q_{tr} - 3G\Delta\varepsilon_d^p$	$q \leftarrow q_{tr} - 3G\Delta\varepsilon_d^p$	$q \leftarrow q_{tr} - 3r\bar{K}\Delta\varepsilon_d^p$
	$\tilde{C}^e$ from $(53)_1$	$\tilde{C}^e$ from $(54)_1$

Update the hardening variables. For the modified Terzaghi, use:

$p_c(\Delta\varepsilon_v^p, \Delta\varepsilon_v^*)$ from (69);

$\vec{H}^p$ from (71) and $(74)_1$.

Yield criterion:

IF $\Phi = \Phi(\vec{\sigma}, p_c)$ THEN compute $\Phi\left(\vec{\sigma}, p_c\right)$, $\frac{\partial\Phi}{\partial\vec{\sigma}}$ and $\frac{\partial\Phi}{\partial p_c}$.

ELSE

Assert the elasticity model is not INhE (combination not handled in the framework)

IF $q_{tr} \approx 0$ THEN

$\boldsymbol{\sigma} \leftarrow p\,\boldsymbol{I}$

ELSE

$\boldsymbol{\sigma} \leftarrow p\,\boldsymbol{I} + \sqrt{\frac{2}{3}} q\,\hat{\boldsymbol{n}}$

Compute $\Phi\left(\boldsymbol{\sigma}, p_c\right)$, $\frac{\partial\Phi}{\partial\vec{\sigma}}$ and $\frac{\partial\Phi}{\partial p_c}$.

Flow rule:

Compute $\vec{N}\left(\vec{\sigma}, p_c\right)$, $\frac{\partial\vec{N}}{\partial\vec{\sigma}}$ and $\frac{\partial\vec{N}}{\partial p_c}$.

Compute the residual and tangent operator:

$\vec{r}$ from (93), $\tilde{M}_{\varepsilon^p}$, $\tilde{M}_\sigma$ and $\vec{V}$ from (97, 98) and $\tilde{J}$ from (96).

3: Check convergence and consistency

IF $\|\vec{r}\| \leq tol$ THEN

IF $\Delta\vec{\varepsilon}^p \cdot \vec{N} > 0$ THEN RETURN

ELSE ERROR

4: Solve the linearized system and update $\Delta\vec{\varepsilon}^p$

$\Delta\vec{\varepsilon}^p \leftarrow \Delta\vec{\varepsilon}^p - \tilde{J}^{-1}\vec{r}$

Update the iteration counter

$i \leftarrow i + 1$

5: GOTO 2: